Comparison of heat transfer and fluid flow characteristics between submerged and free surface jet impingement for two-phase flow

by

Victoria J. Rouse

Submitted in Partial Fulfillment of the Requirements

for the Degree of

Master of Science in Engineering

in the

Mechanical Engineering

Program

YOUNGSTOWN STATE UNIVERSITY

December, 2018

Comparison of heat transfer and fluid flow characteristics between submerged and free surface jet impingement for two-phase flow

Victoria Rouse

I hereby release this thesis to the public. I understand that this thesis will be made available from the OhioLINK ETD Center and the Maag Library Circulation Desk for public access. I also authorize the University or other individuals to make copies of this thesis as needed for scholarly research.

Signature:

_____

Victoria J. Rouse, Student Date

Approvals:

_____

Dr. Kyosung Choo, Thesis Advisor Date

_____

Dr. Hazel Marie, Committee Member Date

_____

Dr. Kevin Disotell, Committee Member Date

_____

Dr. Salvatore A. Sanders, Dean of Graduate Studies Date

ABSTRACT

Impinging jets have been studied in great depth due to their high rates of heat transfer and wide range of application. Some applications of impinging jets include electronic equipment cooling, metal annealing, furnace heating, and many others. The goal of this research was to understand the effects of the nozzle-to-plate spacing and volumetric quality on the Nusselt number of two-phase, free surface impinging jets and submerged impinging jets. The Nusselt number of two-phase, free surface and submerged impinging jets were obtained at several nozzle-to-plate spacings and the trends of the stagnation pressure and Nusselt number were compared. The Nusselt number of the submerged jet was also compared to that of the free surface jets with the same conditions. The two working fluids of the jet were water and air. The nozzle-to-plate spacing ranged from $H/d = 0.03 - 8.5$ and the experiment was done at five volumetric qualities.

The Nusselt number and stagnation pressure decreased exponentially in both free surface and submerged jets for all volumetric qualities in Region I, the jet deflection region. In Region II, the transition region, the Nusselt number and stagnation pressure of the free surface jet remained constant with some fluctuation. The Nusselt number and stagnation pressure of the submerged jet continued to decrease linearly. In Region III, the free jet region, the Nusselt number and stagnation pressure increased linearly in the free surface jet and decreased linearly in the submerged jet.

Comparing the values of the free surface and submerged jet, the submerged jet had a higher Nusselt number for low nozzle-to-plate spacings, and a lower Nusselt number for higher nozzle-to-plate spacings.

CONTENTS

NOMENCLATURE

A	surface area [m^2]
B	width of slot jet [m]
d	diameter of circular nozzle [m]
H	nozzle-to-plate height [m]
h	convection heat transfer coefficient [W/m^2K]
k	Thermal conductivity [W/mK]
L_c	characteristic length [m]
Nu	Nusselt number [-]
P_{stag}	pressure measured at stagnation point [kPa]
p'	fluctuation [Pa]
Q	volumetric flow rate [m^3/s]
Re	Reynolds number [-]
r	radial distance from jet axis [m]
T	temperature [K]
z	axial distance [m]
β	volumetric quality [-]

Subscripts

cond	conduction
conv	convection
w	water
s	surface
stag	measurement taken at stagnation point
∞	surrounding fluid

Superscripts

*	Dimensionless number

Auxiliary

$\dot{Q}$	heat transfer rate

Acronyms

PIV	Particle Image Velocimetry

LIST OF FIGURES

CHAPTER 1

INTRODUCTION

Impinging jets have been studied in great depth due to their high rates of heat transfer and wide range of application. Some applications of impinging jets include electronic equipment cooling, metal annealing, furnace heating, and many others [1, 2, 3, 4]. An impinging jet is a fluid flow that is directed by a nozzle and impinges upon a surface as shown in Figure 1.

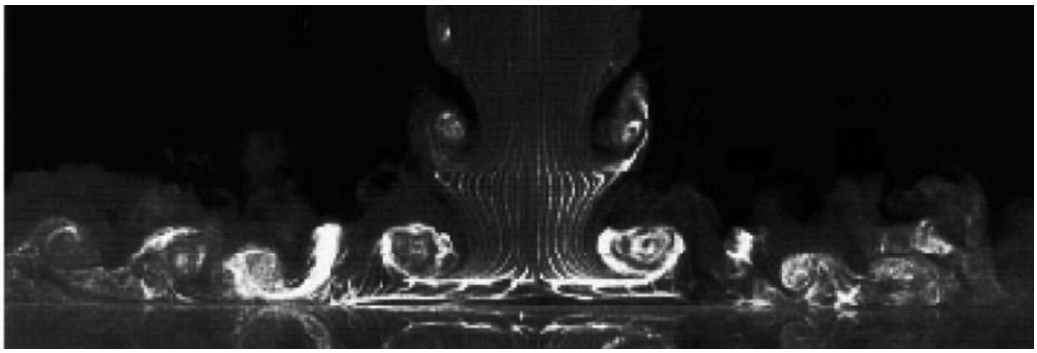

Figure 1: Smoke wire flow visualization of the axisymmetric jet [5].

Impinging jets are widely used in many engineering applications, especially for the heating and cooling of surfaces. They are often favored because of their high heat transfer rates, especially at low nozzle-to-plate spacing.

In the case of this research, the impinging jet studied was submerged, therefore, the jet passed through water before impinging on the surface. The flow of the jet was two-phase, and was made up of air and water. This study focuses on comparing the heat transfer and fluid flow characteristics of a two-phase submerged impinging jet with that of a free surface jet. The Nusselt number of the jet is obtained experimentally at multiple nozzle-to-plate spacings, ranging from $0.03 < H/d < 8.5$. The stagnation pressure and pressure fluctuation are also obtained at the same nozzle-to-plate spacings to understand their relationship to the Nusselt number. This relationship is examined at multiple volumetric qualities of the two-phase flow, ranging from $\beta = 0.1 - 0.9$. Based on the experimental results, the stagnation pressure was found to affect the Nusselt number at varied nozzle-to-plate spacings and volumetric qualities.

Because the impinging jet is known for its high heat transfer rates, it is important to understand what is meant by heat transfer. Heat transfer rate is the rate at which energy in the form of heat is transferred from one system to another as a result of temperature difference. Convection is the mode of energy transfer between a solid surface and the adjacent liquid or gas that is in motion. Forced convection occurs when the fluid is forced to flow over the surface by external means such as a fan, pump, or the wind. Impinging jets use forced convection as a means of heat transfer. The rate of convection heat transfer is well known to be expressed by Newton's law of cooling as:

$$\dot{Q}_{conv} = hA_s(T_s - T_\infty) \tag{1}$$

where h is the convection heat transfer coefficient (W/m^{2}K), A_s is the heat transfer surface area (m^2), T_s is the surface temperature (°C), and T_∞ is the fluid temperature (°C). The convection heat transfer coefficient h is an experimentally determined parameter that is determined based on the geometry, nature of the fluid motion, properties of the fluid, and the bulk fluid velocity. From Newton's law of cooling, the convective heat transfer coefficient can be defined as the rate of heat transfer between a solid surface and a fluid per unit surface area, per unit temperature difference. Experimentally, it can be determined if the surface area, surface temperature, surrounding temperature, and rate of heat transfer of a system are known:

$$h = \frac{\dot{Q}_{conv}}{A_s(T_s - T_\infty)} \tag{2}$$

When studying the heat transfer of an impinging jet, it is important to know how the convection in a fluid layer enhances the heat transfer relative to the conduction across the same fluid layer. The conductive heat transfer of a system can be defined with Fourier's law:

$$\dot{Q}_{cond} = -kA\frac{(T_s - T_\infty)}{\Delta x} \tag{3}$$

where k is the thermal conductivity of the fluid (W/mK), A is the surface area (m^2), T_s is the surface temperature (°C), and T_∞ is the fluid temperature (°C). A convenient way to look at convective heat transfer rate relative to conductive heat transfer rate is to look at the dimensionless ratio between the two rates, known as the Nusselt number:

$$Nu = \frac{hL_c}{k} \tag{4}$$

where L_c is the characteristic length (m). Impinging jets undergo heat transfer due to convection and conduction. The Nusselt number is the method used for comparing the two. A higher Nusselt number indicates that more of the heat transfer is taking place due to convection.

There are many types of jets, types of flow, types of nozzle, and angles of impingement to be found among impinging jets. Therefore, some distinctions will be made. There are two types of impinging jets, *free surface jets*, and *submerged jets*. In a free surface jet the jet ejects into a gaseous environment before impinging on a surface, where the entrainment of the surrounding fluid is minimal. In a submerged jet, the jet ejects into a fluid of the same state before impinging on a surface, where the entrainment of the surrounding fluid is significant [6]. In the present study, the submerged jet will be considered, and the surrounding fluid is water. There has been a large amount of study on single-phase impinging jets, where the fluid in the jet consists of fluid in only one phase, usually liquid. In this study however, two-phase flow was considered, where the jet is composed of two phases of fluid simultaneously [7]. The two fluids are water and air. The flow physics of an impinging jet also depends on the design of the nozzle. In this study, a circular nozzle will be considered, which produces axisymmetric velocity profiles, as opposed to a slot jet, which is another commonly used impinging jet. Finally, the angle of impingement is important to consider. In the current study, the angle between the jet and the impinged surface is 90°. Now that some distinctions have been made about the type of jet being described, some statements about the physics of impinging jets can be made.

CHAPTER 2

BACKGROUND

One of the first studies on the heat transfer rates of impinging jets was done by Friedman and Mueller in 1951 [8]. This study obtained heat transfer coefficients of a point on a target plane made of rigid plastic insulating material. Copper-constantan thermocouples were inserted into holes drilled at several radii from the jet center. The target was heated by a furnace. The results were limited to laminar flows until Gardon developed the Gardon gauge to measure heat transfer coefficient profiles over the surface [9]. These heat flux sensors were small and precise, and allowed accurate measurement of heat transfer at a point and could withstand high heat fluxes [10]. The Gardon gage was used to measure the radial profiles of the heat transfer coefficient of an impingement surface. Gardon and Cobonpue [9] showed the profile of the heat transfer coefficient for a circular impinging jet as extending outward radially from the stagnation point along the impinging surface depends strongly on the nozzle-to-plate spacing. The profiles included measurements from directly under the jet, and extending outward along the impinged surface. The results are shown in Figure 2. An interesting feature of this research is that, for a large nozzle-to-plate spacing, the highest heat transfer rate occurs directly under the jet, at the stagnation point, but as the nozzle-to-plate spacing decreases, the highest heat transfer rate occurs slightly offset from the stagnation point, and a local minimum heat

transfer rate occurs at the stagnation point. At lower nozzle-to-plate spacings, there appears two radial peaks in the heat transfer rate immediately surrounding the stagnation point one at $r/d \approx 0.5$, and one at $r/d \approx 2$. The first at $r/d \approx 0.5$ correspond to high radial velocities, and the second is explained as a result of the hydraulic jump that surrounds the impinging jet. In 1965, Gardon and Akfirat [11] used this same method to study the effect of turbulence on an impingement surface. This study showed that the intensity of the turbulence is effected by the Reynolds number and the normalized nozzle-to-plate spacing H/B, where B is the width of a slot jet, and the liquid only Reynolds number is defined as:

$$Re_w = \frac{4Q}{\nu \pi D} \tag{5}$$

This experiment also explained the local minimum of heat transfer rate at the stagnation point and the outer peaks of heat transfer rate at lower nozzle-to-plate spacing as being caused by transition from laminar flow to turbulent in the jet, implying that the flow conditions upstream are important to consider in low nozzle-to-plate spacing.

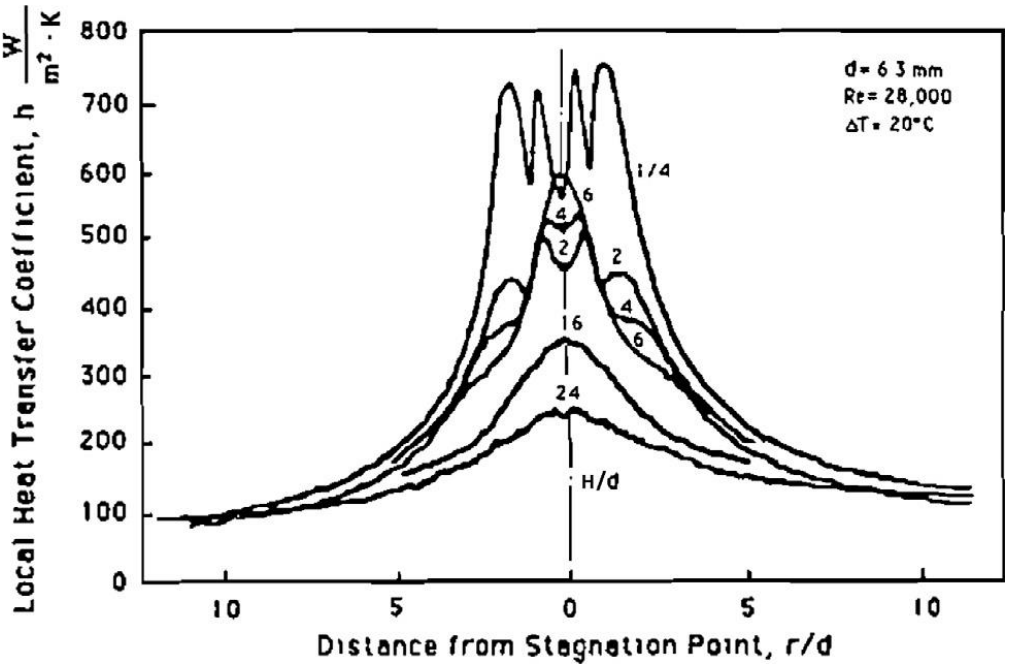

Figure 2: Radial profile of heat transfer characteristics at multiple nozzle-to-plate spacings [9].

More recently, some methods of studying heat transfer characteristics of impinging jets have become common in the field. One common method is to use liquid crystals as a sensing element [12] [13]. Heat transfer data is obtained visually, since the crystals change colors to indicate temperature changes [10]. The first to do this was R.J. Goldstein, J.F. Timmers [14]. They were able to confirm the local minimum at the stagnation point, at low nozzle-to-plate spacings. The authors attribute this to the fact that impingement is taking place within the potential core, or the center of the jet where there is not yet turbulence generation due to mixing. Another method that has become popular is to use infrared (IR) thermography to produce a thermogram with the temperature contours of the impinging plate [15] [16] [17]. A successful use of this experimental set up by G.M. Carlomagno [18] showed the local minimum at the stagnation point of the impingement surface, the inner maximum at about $r/d = 0.5$, and the outer maximum at $r/d = 1.5$. A later use of this

method by Lytle and Webb [19] not only confirmed this local minimum and maximum heat transfer value at low nozzle-to-plate spacing, but showed the location of the maximum value coincides with the maximum value of turbulence fluctuation. Another popular method for analyzing fluid flow and heat transfer characteristics of impinging jets is particle image velocimetry (PIV) [20] [21] [22]. Hammad and Milanovic [23] aimed to characterize the turbulent flow structure of the nozzle in the impingement and wall-jet regions using PIV. Their results showed the profiles of the velocity in the axial direction and the radial direction. Recent studies have included theoretical modeling. Modak et al. [24] conducted theoretical studies on the heat transfer characteristics of a two dimensional impinging jet between 1 and 10 nozzle diameters away from the impingement surface. A generalized expression was obtained that included several modelling parameters such as Nusselt number, nozzle-to-plate spacing, Prandtl number, Reynolds number, and the modelling parameter k. An infrared thermal imaging camera was used to obtain experimental results which were compared to theoretical results. The theoretical results were also compared to experimental results of many other studies. In the study, the theoretical predictions were able to predict the experimental results within an error band of 10%. Though much about the impinging jet has been studied over the years, even so, the impinging jet will likely be a subject of investigation for a long period of time, since in real life applications, the geometries are often complex and consists of multiple jets interacting, and may impinge at different angles, with jets being composed of a wide array of fluids.

2.1 Physics of Impinging Jets

Because of the high heat transfer rates of impinging jets, many studies have been focused on the heat transfer characteristics of impinging jets, especially single-phase and free surface jets. It is important to have an understanding of the research already done on impinging jets. The experimental contributions to the knowledge of submerged jets (generally single phase flow) and the experimental contributions to the knowledge of two-phase flow (generally free surface jets) are explored further. The experimentation of this study focuses on two-phase flow in submerged jets.

2.1.1 Submerged Impinging Jet Flow Physics

The description of submerged impinging jet flow starts at the nozzle exit and moves along the axis of the nozzle towards the impinged surface (axial direction) and then moves along the impingement surface (radial direction). The flow along each of these paths can be divided into several regions. The lengths of these regions depend on the nozzle-to-plate spacing and the nozzle diameter. The nozzle-to-plate spacing can be large or small relative to the nozzle diameter, so the dimensionless H/d is used when referring to nozzle-to-plate spacing, where H is the height of the nozzle from the plate or distance between the nozzle and plate, and d is the nozzle diameter. H/d normally refers to the distance between the nozzle exit and the impingement surface. In general, when referring to locations of phenomena that that depend on the location of the nozzle, such as the potential core, the distances are expressed in nozzle diameters which are measured from the nozzle exit unless otherwise stated. This is not to be confused with the measurement z/d, which is a measure

of the distance above the impingement surface, and is used to refer to a place along the z-axis, or the jet axis, regardless of the nozzle-to-plate spacing. The measurement *z/d* is used when referring to phenomena that do not depend on the location of the nozzle, such as the length of the stagnation region. When describing the regions of flow, it is important to differentiate between large and small nozzle-to-plate spacing. The flow regions are described by Carlomagno [10]. The regions of flow of large nozzle-to-plate spacing will be described first. Each region can be seen in Figure 3.

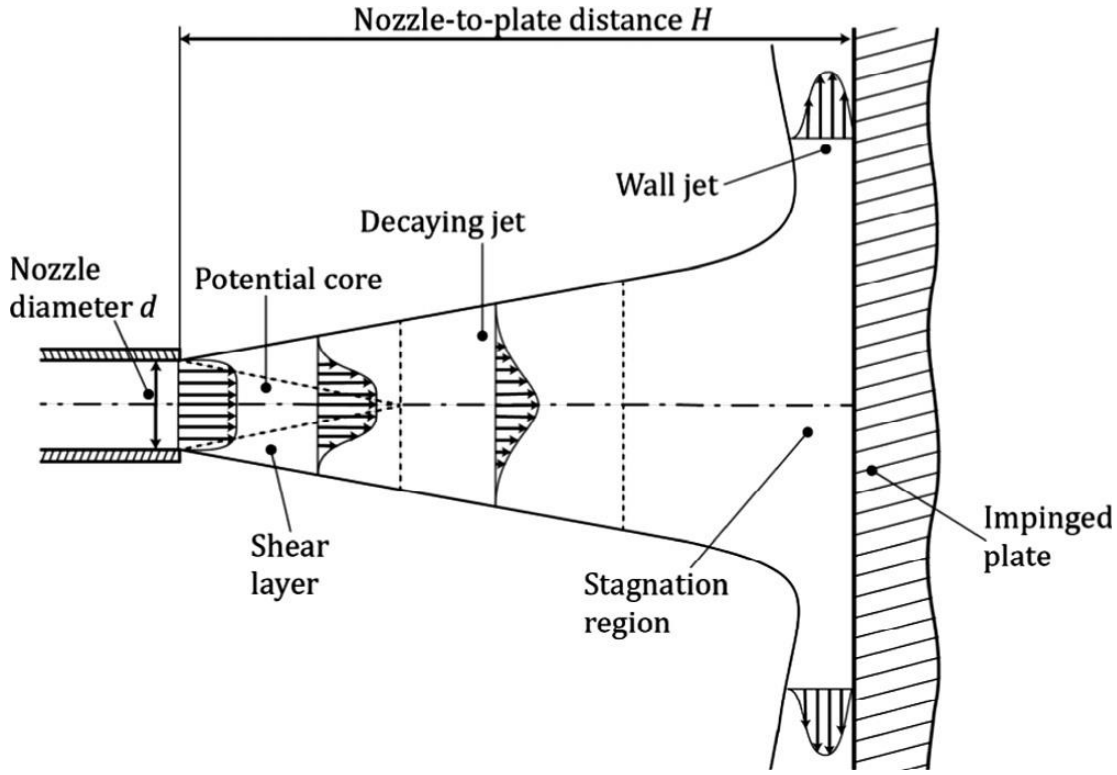

Figure 3: The flow regions of a submerged impinging jet [10].

Upon exiting the Nozzle, the jet has a defined velocity and temperature profile and turbulence characteristics dependent on the conditions of the flow upstream [25]. At a large

nozzle-to-plate spacing, the jet emerging from the nozzle is sufficiently far from the impingement surface, and therefore behaves as a free submerged jet. This region is sometimes called the *free jet region*. The free jet region extends to the stagnation region, and can be divided into several parts. As the fluid emerges from the nozzle, the difference in velocity between the free jet and the surrounding fluid results in a shear driven interaction. Because the interaction is between two fluids at two velocities, the jet begins to entrain the surrounding fluids into the flow causing the jet radius to widen. As the shear layer of the jet entrains the surrounding water, mixing occurs between the two layers and this mixing generates turbulence. The radial velocity profile of the jet also becomes non-uniform as the shear layer of the jet experiences a decrease in velocity due to the surrounding water. The interaction with the surrounding water results in an increase in the mass, momentum, and energy of the outside layer of the jet. The jet as a whole, however, begins to lose energy and decrease in velocity as the velocity profile widens.

Though the shear layer of the jet is widening in the free stream, the interior of the jet maintains its original flow velocity and pressure close to the nozzle. Its velocity profile also remains intact close to the nozzle and is generally uniform across the flow surface area. As the jet interacts with the surrounding fluid, the velocity as a whole begins to decrease. The decrease of velocity starts on the shear layer of the jet and gradually diffuses inward, until eventually, the jet velocity as a whole is decreased. The interior part of the jet which remains intact is called the *potential core*. As the shear layer is widening, the potential core becomes thinner until it vanishes. The length of the potential core depends on the turbulence of the flow and the initial velocity at the nozzle. Livingood and Hrycak [26] show the length of the potential core to be 6-7 nozzle diameters in length. Gardon and

Akfirat [11] showed the potential core of a slot jet to extend approximately 5 slot widths. It can also be defined as the axial position from the nozzle where the average centerline flow dynamic pressure reaches 95% of its initial value [10].

The region after the potential core is the *decaying jet region*, and can be split into two parts, the *flow developing region* and the *fully developed region*. The velocity at the axis of the decaying jet decreases due to the entrainment of the surrounding water. Both the potential core and the decaying jet region are combined to form the *free jet region*. The free jet region is sufficiently far from the impingement surface and is not affected by it.

As the flow approaches the plate, it exits the free jet region and enters the *stagnation region*, named because the flow is approaching the stagnation point, and the flow no longer behaves as a free submerged jet, but is now influenced by the impingement surface. The stagnation point is located on the impingement surface at the center of the jet axis. As the flow moves towards the stagnation point, the static pressure increases rapidly. The axial velocity component is simultaneously decreasing due to the high static pressure build up at the impingement surface. The axial velocity eventually decreases to zero at the impingement surface. Once the flow passes the stagnation point the velocity becomes almost completely radial. The pressure begins decreasing again as the flow increases its radial velocity along the impinged plate. Schrader [27] and Leclerc [28] independently determined the length of the stagnation region to be about 1.2 nozzle diameters in length, starting at the stagnation point on the impingement surface and progressing upwards towards the nozzle; in other words, deceleration begins 1.2 nozzle diameters above the impingement surface. The stagnation zone has a radius of approximately 1.1 nozzle diameters according to Schrader [27]. Within this radius on the impingement surface the

boundary layer maintains a constant thickness. In their study, Hammad and Milanovic [23] showed the variation of the mean axial velocity along the z-axis. The mean axial velocity is measured at z/D values ranging from 0 -1 where z is the distance from the impingement surface and D is the nozzle diameter. The mean axial velocity is shown to drop slightly near z/D values of 1, and the author attributes this to turbulent shear stress and increased distance from the nozzle. Further downstream, at lower z/D values, the velocity begins to drop more rapidly. Their results can be seen in Figure 4.

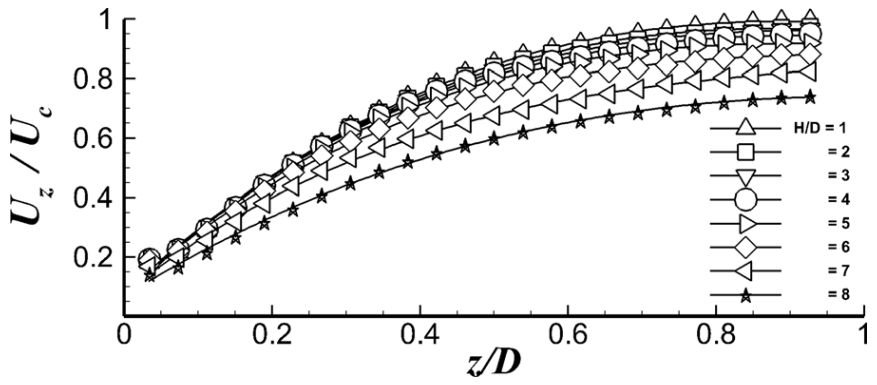

Figure 4: Mean axial velocity Uz/Uc decay along z-axis for given separation distances H/D [23].

After the flow passes the stagnation region, it spreads radially outward, with its velocity almost completely parallel to the impingement surface. This is called the *wall jet region* [29]. The radial velocity of the flow in this region starts at zero at the stagnation point and gradually accelerates to some maximum value. According to Abramovich [30] this maximum value occurs at a radial distance of about one nozzle diameter away from the stagnation point. The boundary layer thickness at the impingement surface begins to grow as the flow moves along the impingement surface. As the flow moves along the wall

jet region, it now has two surfaces with which a velocity gradient is created due to no slip conditions. One is at the impingement surface, and one is at the interface between the flow and the surrounding water. The boundary layer thickness of the jet along the wall from this point can be defined as the height where the mean "wall-parallel" velocity component is maximum at a given radial position. Because the jet is completely submerged in water, several things happen to the flow. It continues to entrain the surrounding water as it moves along the wall jet region, therefore, it is increasing in height relative to the impinged surface. The jet eventually dissipates and the fluid becomes a part of the surrounding fluid. Hammad and Milanovic [23]were able to show this in their PIV experiment. Their results are referenced in Figures 5 and 6.

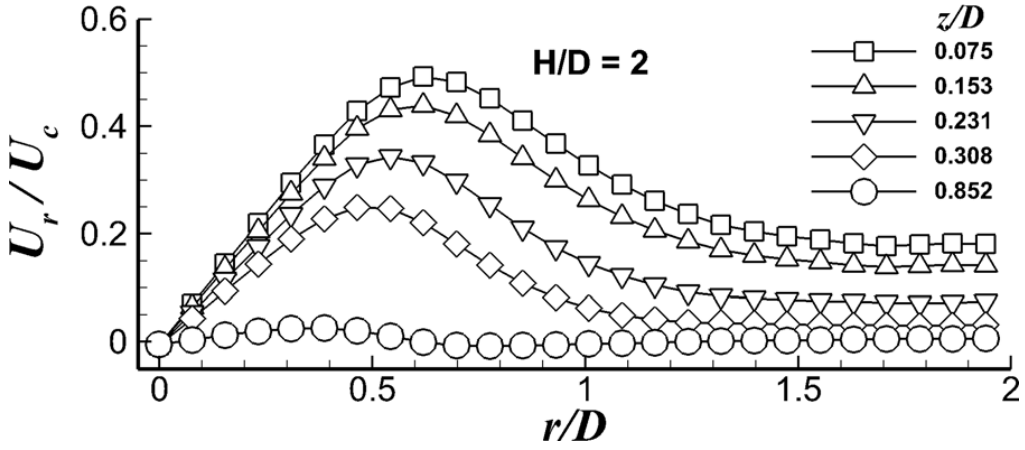

Figure 5: Mean radial velocity profiles at different axial distances from the impingement plate r/D [23].

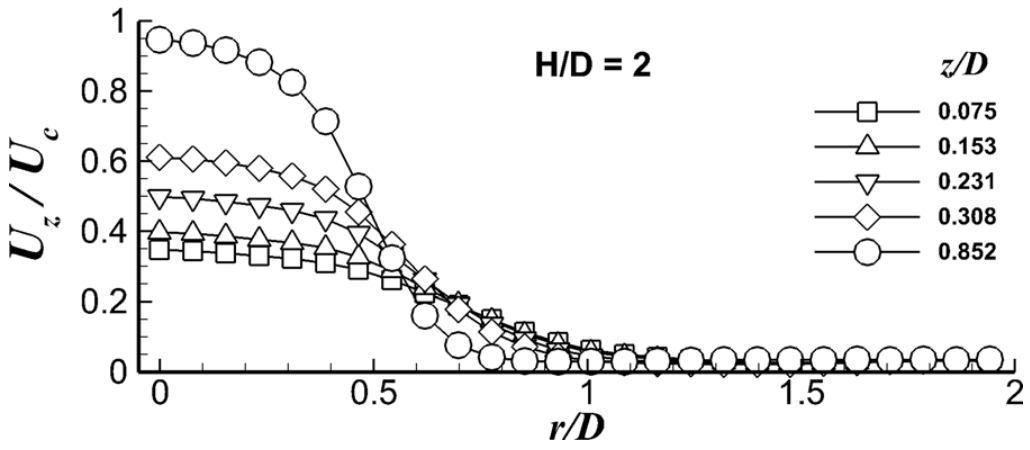

Figure 6: Mean axial velocity profiles at different axial distances from the impingement plate r/D [23].

Figure 5 shows the mean radial velocity profiles for a jet with a nozzle-to-plate spacing of $H/D = 2$ starting at zero at the jet axis and increasing due to the deflection of the jet. The velocity reaches some maximum value, which differs at various distances z/D, and then begins to decrease. The mean axial velocity at the jet axis shown in Figure 6 varies depending on the distance from the impinging surface. As the distance from the jet axis increases, however, the axial velocity decreases and approaches zero.

The physics of the submerged jet changes as the nozzle-to-plate spacing decreases. Because the flow has less space, some of the previously described regions are not able to develop. The fully developed region of the decaying jet region is the first to disappear and then the whole decaying jet region disappears as the nozzle-to-plate spacing decreases. If the nozzle is within two nozzle diameters, the decaying jet region disappears entirely, and the potential core will begin to overlap the stagnation region. High static pressure buildup of the stagnation region will affect the flow at the nozzle exit, and will change the shape of the potential core as the nozzle-to-plate spacing gets smaller. At small distances (H/d), impingement happens within the jet potential core and a velocity profile will develop less

and less. The velocity profile will be almost uniform as it impinges upon the surface. Less turbulence generation due to mixing takes place, and the shear layer does not expand into the potential core.

A study by Choo [31] shows the influence of nozzle-to-plate spacing on heat transfer and fluid flow characteristics. The results can be divided into three regions. In region I, the jet deflection region ($0.1 < H/d < 0.6$), the normalized stagnation Nusselt number and dimensionless stagnation pressure drastically increase with decreasing the nozzle-to-plate spacing. In region II, the potential core region, ($0.6 < H/d < 7$), the effect of the nozzle-to-plate spacing is negligible on the normalized stagnation Nusselt number and pressure since the average velocity of potential core is constant. In region III, the free jet region, ($7 < H/d < 40$), the normalized stagnation Nusselt number and pressure monotonically decrease with increasing the nozzle-to-plate spacing due to a decrease in jet velocity.

2.1.2 Two Phase Flow—the Role of Turbulence

It is well known that the addition of gas to a liquid impinging jet enhances the heat transfer rate. Zumbrunnen and Balasubramanian [32] observed an increase in the heat transfer rate of liquid-only impinging jets by a factor of 2.2 when the Reynolds number was between $3700 \leq Re_w \leq 21{,}000$ and a volumetric fraction was $0 \leq \beta \leq 0.86$. Serizawa [33] observed an increase in the heat transfer coefficient by a factor of two when studying circular jet with an air-water mixture and a Reynolds number between $25{,}000 \leq Re_w \leq 125{,}000$ and a volumetric fraction of $\beta = 0.53$. Friedrich [34] studied impinging

jets with volumetric qualities varying from $0 < \beta < 0.9$ and Reynolds number varying from $3{,}030 < Re < 4{,}329$. It was shown that the highest Nusselt number value was attained at $\beta = 0.8$. Based on these studies, it can be concluded that the addition of gas into a liquid only jet increases the heat transfer characteristics. Lytle and Webb [19] observed the heat transfer characteristics and flow structure of impinging air jets at low nozzle-to-plate spacings. The fluid acceleration and increase in turbulence found in the nozzle plate gap was found to cause an increase in the heat transfer characteristics. This study also showed a local maximum of the turbulence in the same location as the local maximum in heat transfer. Trainer et al. [35] showed that the heat transfer of air assisted jets was enhanced by a factor of 2.6. Hall et al. [36] showed that heat transfer increased by a factor of 2.1 on air-water impinging jets with volumetric qualities ranging from $0 < \beta < 0.4$, and liquid only Reynolds number ranging from $11{,}300 \leq Re_w \leq 22{,}600$. Chang et al. [37] found an enhancement by a factor of 1.2 on confined, liquid-vapor impinging jets composed of Freon R-113 relative to single phase jets. This suggests that turbulence effects the heat transfer characteristics of impinging jets.

In a single-phase flow through a pipe, the flow is considered to be either laminar or turbulent based on its Reynolds number. The Reynolds number of an impinging jet after it exits the nozzle is based on the nozzle diameter, and other exit conditions. There is no direct evidence confirming a definite transitional Reynolds number [38]. A commonly accepted Reynolds number value below which flow is considered laminar is 2500 [39]. Turbulence is generated in an impinging jet after the flow exits the nozzle. This is because the mixing that occurs between the jet and the surrounding fluid, (whether liquid or gas) generates turbulence. This turbulence can be up to 30% more intense than the turbulence

in pipe flow [40]. The typical increase of turbulence and corresponding decrease in center-line velocity of an impinging jet can be seen in Figure 7, where $\frac{u_m}{u_e}$ is the center-line velocity and $\frac{u'}{u_m}$ and $\frac{u'}{u_e}$ are the intensity of the turbulence.

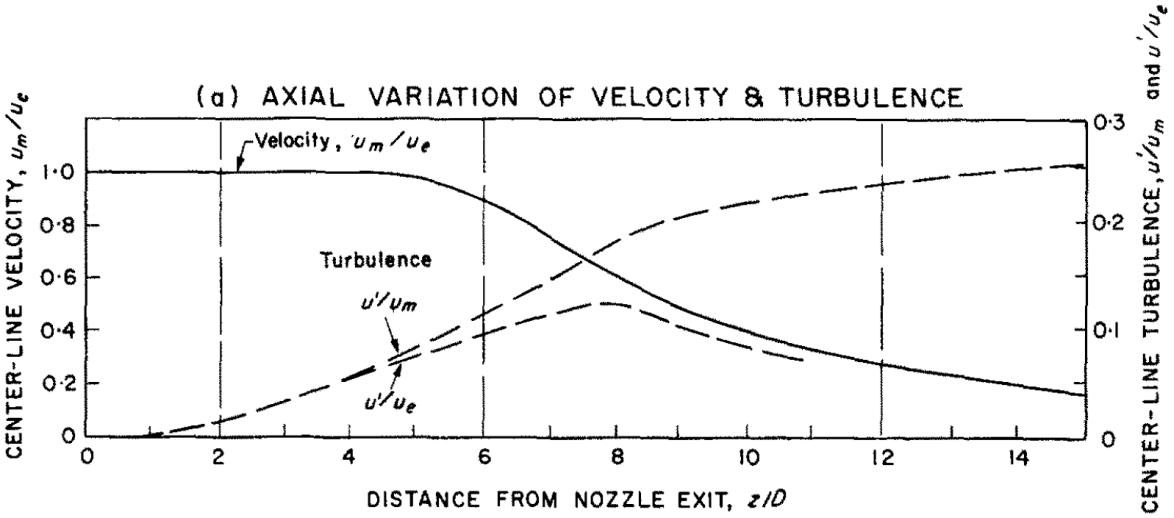

Figure 7: Increase in turbulence and decrease in center-line velocity of an impinging jet [40].

A single phase flow can start as laminar flow at the nozzle exit and become turbulent before it reaches the impingement surface due to the interaction between the jet and the surrounding fluid [10]. Whether or not a laminar flow becomes turbulent depends on the original velocity profile and the nozzle-to-plate spacing, which affect the mixing at the shear layer of the jet. Flow may also begin as turbulent before it exits the nozzle. In this case, the mixing of the jet and the surrounding fluid generates more turbulence in the jet. In either case, the mixing generates turbulence in the jet [10]. The intensity of the turbulence generated by mixing depends on the destabilizing effects of the shear forces and the stabilizing effects of fluid viscosity. The turbulence of the flow as it impinges on the

plate affects the heat transfer characteristics, therefore it is important to understand the affects that turbulence has on single-phase flow in order to see how it can effect two-phase flow.

A common range of Reynolds numbers (based on nozzle diameter) for single-phase circular free jets according to McNaughton et al. can be seen in Table 1 [41]. These values vary slightly in other studies.

Table 1: Reynolds number for circular impinging jets [41].

Center	Off-set
Dissipated laminar jet	$Re < 300$
Fully laminar jet	$300 < Re < 1000$
Transitional or semi-turbulent jet	$1000 < Re < 3000$
Fully turbulent jet	$Re > 3000$

For low Reynolds numbers, ($Re \cong 450$) the jet remains laminar throughout its entire length, and turbulence has no effect on the heat transfer characteristics [11]. In this case, the Nusselt number remains constant as long as the jet is impinging within the potential core and diminishes proportionally to H/d beyond that [11]. On the other hand, if $Re > 2750$, the jet is turbulent on emerging from the exit and will become more turbulent as the flow progresses and interacts with the surrounding fluid. This increase in turbulence begins at $z/B = 1$, and continues to increase, as the jet velocities remain fairly constant inside of the potential core. The increase in turbulence creates an increase in the

heat transfer coefficient at the stagnation point. At $H/d = 5$, where the decrease in velocity begins, and the heat transfer coefficient should begin to decrease with it. However, the effect of the increasing turbulence due to mixing is still dominant, and the heat transfer coefficient continues to increase. As the decrease in velocity continues, the jet width also increases and contributes to the lowering of the heat transfer coefficient. It isn't until $H/d = 8 - 10$ that the decreasing velocity and widening jet radius begin to have a dominant effect on the heat transfer coefficient, thus decreasing it [11].

In a study by Gardon and Akfirat [11], a mesh screen that acted as a turbulence promoter was installed in the nozzle of a submerged impinging jet. The results are shown in Figure 8.

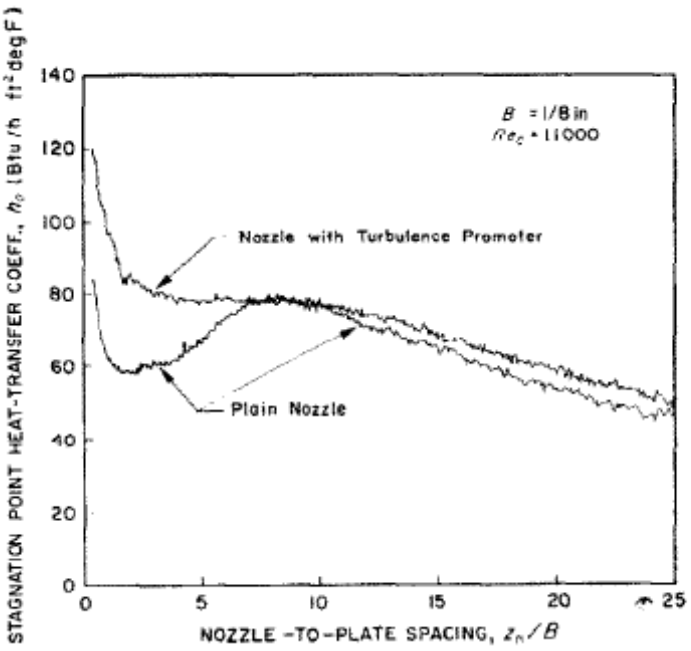

Figure 8: Effect of artificially induced turbulence on stagnation point heat transfer coefficient h [11].

The heat transfer coefficient can be increased by increasing the turbulence of the jet, compared to the values obtained without increasing the turbulence "artificially." The largest differences can be seen at low nozzle-to-plate spacing, where the induced turbulence is still the dominant factor. The effect of the induced turbulence decreases as the distance from the turbulence promoter increases. The increase in heat transfer coefficient is due predominantly to the induced turbulence, and the difference between the heat transfer coefficients of the two nozzles becomes smaller as the distance from the turbulence promoter becomes larger.

In a study by Hofmann [42] the role of turbulence in the flow structure and heat transfer of a free jet are compared to an impinging jet. The free jet was composed of air only, and the surrounding fluid consisted of air only. Under these experimental conditions, the velocity and turbulence intensity profiles were obtained using Laser Doppler Velocimeter. The study first shows profiles for a free jet, at several distances from the nozzle (z/D). The results were then compared to the results of impinging jets, under the same condition. In Figure 9, the left column shows the normalized axial velocity $\overline{u_N}$ profiles and the right column shows the turbulence intensity $\overline{u'_N}$ profiles.

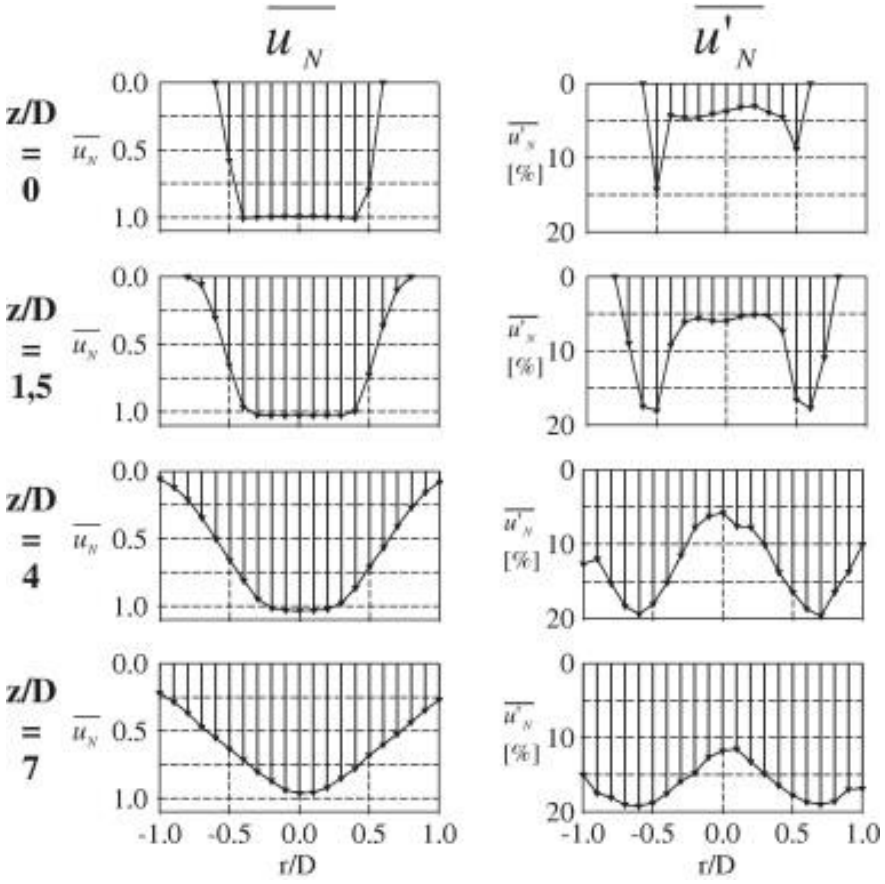

Figure 9: Normalized axial velocity and turbulence intensity profiles in a free jet at four distances from the nozzle [42].

At the nozzle, where $z/D = 0$, the turbulence intensity is approximately 4% of the mean axial velocity at the nozzle exit in the potential core, but it is higher in the boundary region, where the velocity is low. As the nozzle-to-plate spacing is increased, the potential core of the jet becomes smaller, and the turbulence intensity in the boundary layer increases. The radius of the jet becomes larger, but the radius of the potential core becomes smaller. The entrainment of the surrounding air causes the turbulence intensity to increase. In this same study, Hofmann then compares the results to an impinging jet. This was done by choosing the nozzle-to-plate spacing to be large enough that that the free and impinged jet have the same flow structure above an H/D value of 1.2 nozzle diameters. The comparison shows that the velocity and turbulence intensity values are nearly the same.

In a two-phase flow, the flow is a mixture of liquid and gas, and the turbulence intensity can be measured by the fluctuation of pressure or velocity [43]. For turbulent flow, the stagnation pressure is varying randomly as a function of time and space. There is no known solution of the random function $p(x, y, z, t)$. Letting the mean pressure $\bar{p}$, be the time average of the pressure of a turbulent jet, the fluctuation of the pressure is defined as:

$$p' = p - \bar{p} \tag{6}$$

The fluctuation of the pressure for turbulent flow is defined as the deviation from the time average. The mean square of the fluctuation is the intensity of the turbulence [43]. There has been a great deal of study on the effects of pressure on the heat transfer characteristics of impinging jets. With the addition of a second phase into the flow, there

is a need for a study of the effects of the fluctuation of the pressure on the heat transfer characteristics.

Two-phase flow consists of liquid and gas. The volumetric quality (β) of a two phase flow specifies how much of the flow is liquid and how much is composed of gas. The volumetric quality is defined as:

$$\beta = \frac{Q_g}{Q_g + Q_l} \tag{7}$$

where Q_g is the volumetric flow rate of the gas in the mixture and Q_l is the volumetric flow rate of the liquid in the mixture.

As shown by Friedrich [34] increasing the volumetric quality of a two-phase impinging jet at $H/d = 1$ increases the Nusselt number until $\beta = 0.8$, and increasing the volumetric quality higher than this value causes a decrease in Nusselt number. This suggest that increase in volumetric quality increases the Nusselt number until the effects of adding air to the mixture become more dominant and decrease the Nusselt number.

In Figure 10, Friedrich shows the fluid flow patterns of two-phase flow in the nozzle for multiple volumetric qualities, including $\beta = 0.1, 0.2, 0.3, 0.6,$. For $\beta = 0.1, 0.2, 0.3$, the flow exhibits a bubbly flow. For $\beta = 0.6, 0.8$, the flow exhibits a slug pattern. For $\beta = 0.9$, the flow becomes annular.

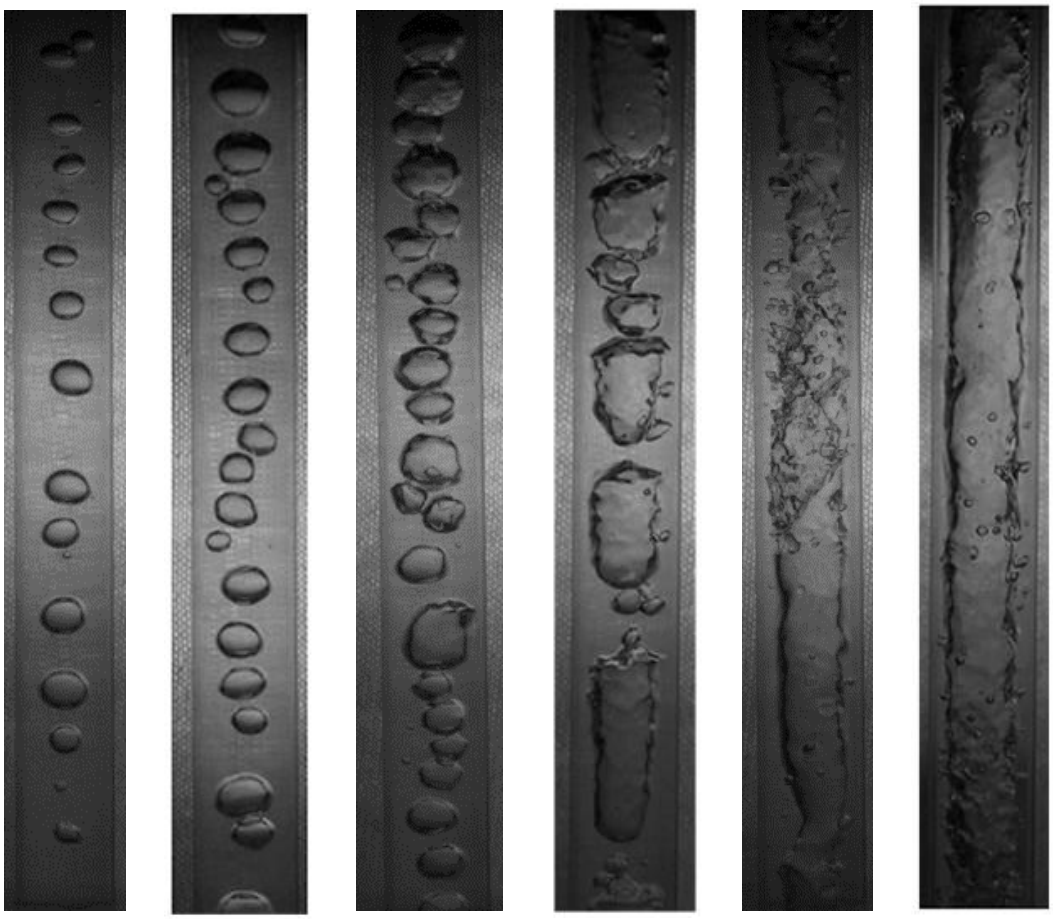

(a) β = 0.1 (b) β = 0.2 (c) β = 0.3 (d) β = 0.6 (e) β = 0.8 (f) β = 0.9

Figure 10: Flow patterns inside of the nozzle for various β at Re = 4,329 [34].

2.2 Scope of Research

The goal of this research is to understand the effects of the nozzle-to-plate spacing and volumetric quality, on the Nusselt number of two-phase, free surface impinging jets and submerged impinging jets. The effects of pressure, and pressure fluctuation were observed. The Nusselt number of free surface and submerged impinging jets were obtained at several nozzle-to-plate spacings and the trends were compared to the trends of the stagnation pressure. The Nusselt number of the two-phase, submerged jet was also analyzed at several nozzle-to-plate spacing, and the values were compared to those of the free surface jets with the same conditions. The two fluids of the jet were water and air. The nozzle-to-plate spacing ranged from $H/d = 0.03 - 8.5$ and the experiment was done at five volumetric qualities $\beta = 0.1, 0.3, 0.5, 0.7, 0.9$. The pressure and the fluctuation of the pressure at the stagnation point was also taken into consideration to understand how they affect the heat transfer characteristics. Based on the experimental results, the relationship between the Nusselt number and the nozzle-to-plate spacing was obtained for five volumetric qualities, for both submerged and free surface jet impingement.

CHAPTER 3

METHODOLOGY

The Nusselt number and stagnation pressure of a two-phase submerged impinging jet with a liquid-only Reynolds number of 3180 were measured at multiple dimensionless nozzle-to-plate spacings ranging from $0.03 < H/d < 8.5$. This was done for 5 volumetric qualities, including $\beta = 0.1, 0.3, 0.5, 0.7, 0.9$. A separate experiment was designed for each of the desired values. In the present chapter, the apparatus and procedure of each of the experimental setups are described.

3.1 Apparatus

The fluid flow experimental setup was designed to measure the stagnation pressure and the heat transfer experimental setup was designed to measure the Nusselt number. The two shared a flow system. The flow system, fluid flow experimental setup, and heat transfer experimental setup are described in the following sections.

3.1.1 Flow System

In order to achieve two-phase flow, air and water each passed through flexible tubes and entered a single tube, where they were mixed, shown in Figure 11. The water was

supplied by a commercial water line in the building. The air flow was supplied by a high-pressure tank, which passed air through a pressure regulator. Both the liquid mass flow rate and air mass flow rate were regulated before mixing to ensure an accurate volumetric quality was maintained. The water flow was regulated by a flowmeter valve (Dwyer RMB-84-SSV). The range of the flowmeter valve was 0-40 GPH. The air was also regulated by two mass flow controllers. The flow controller used depended on the volumetric quality of the mixture. For lower volumetric qualities ($\beta = 0.1, 0.3, 0.5$), the Omega FMA5514A was used. The full scale range of the Omega FMA5514A is $0 - 1000 \frac{mL}{min}$. For higher volumetric qualities ($\beta = 0.7, 0.9$), the Omega FMA5520A was used, and the full scale range is $0 - 10 \frac{L}{min}$. To create the two-phase impinging jet, the two fluids were regulated in separate tubes and then combined in a single nozzle. A schematic can be seen in Figure 12. The volumetric quality was controlled by keeping the flow rate of the water constant at $1.4721 \times 10^{-5} \frac{m^3}{s}$ throughout the experiment, and varying the air flow rate in order to change the volumetric quality.

Figure 11: Two-phase mixer. Two fluids are combined in a single nozzle.

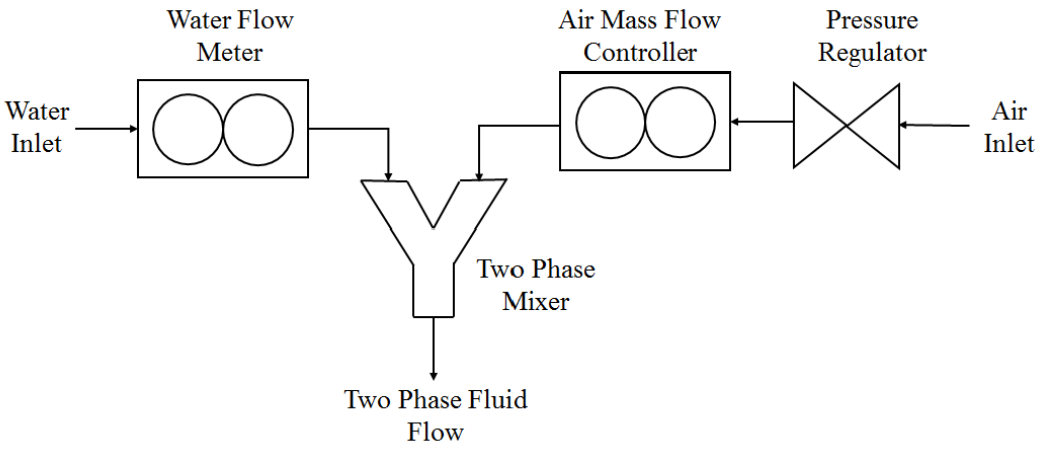

Figure 12: Schematic of the flow system to create two-phase flow for air and water [34].

The nozzle in which the fluids were combined was 470mm long, and was made of extruded acrylic. The nozzle had a diameter of 5.86mm. The nozzle was circular, producing an axisymmetric velocity profile. The nozzle was mounted on a 3-axis stage (x, y, z,),

(Thorlabs, Inc, PT3A/M) that had a resolution of $10\ \mu m$. The mounted nozzle can be seen in Figure 13. Once the nozzle was mounted on the stage, the nozzle-to-plate spacing could be varied by raising and lowering the z-axis control in between each data point. The z-axis control can also be seen in Figure 13. The range of the stage was $0 - 25mm$. In order to attain H values larger than $25mm$, the nozzle was manually moved in line with markings on the side of the tank which can be seen in Figure 14.

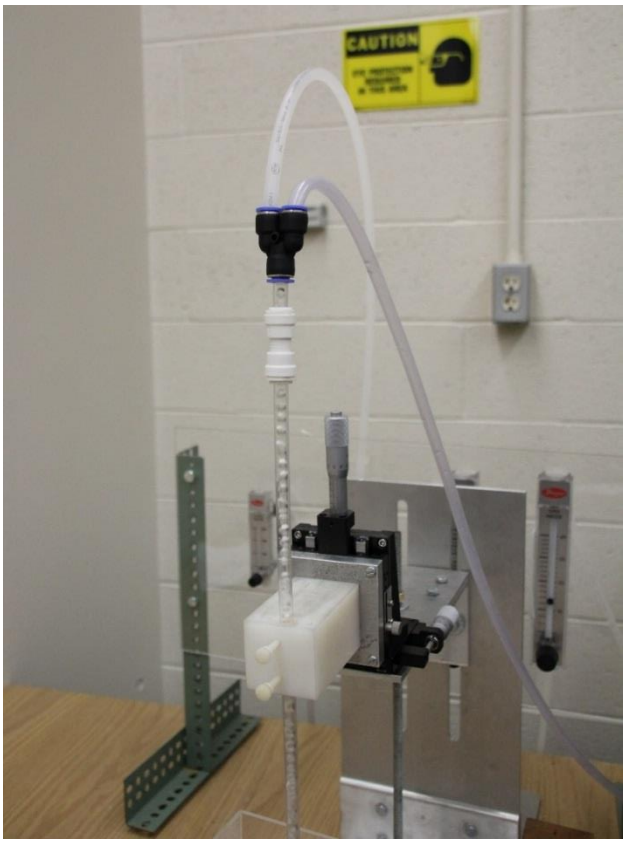

Figure 13: Nozzle mounted on 3-axis stage.

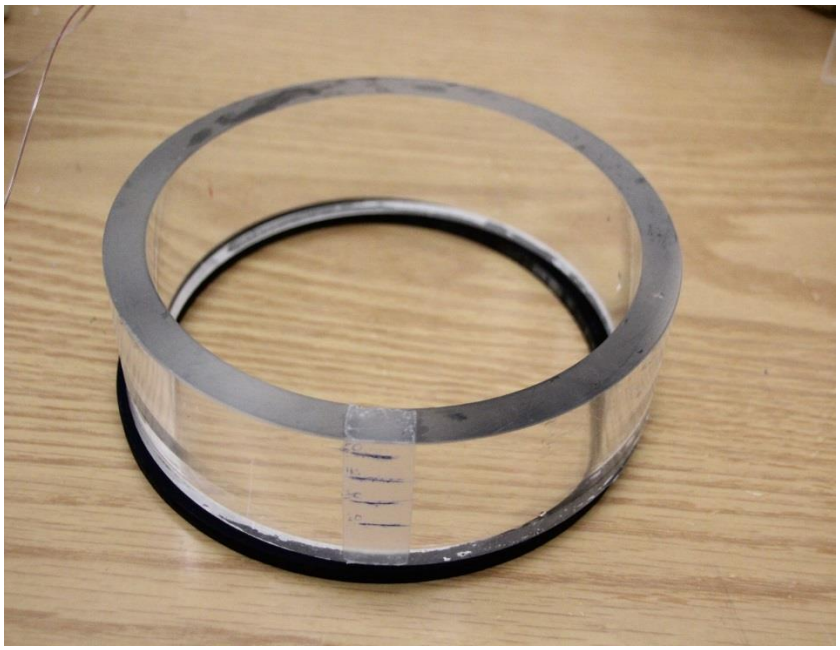

Figure 14: A cylindrical tank used to achieve a submerged jet can be lifted to achieve a free surface jet. The tank has markings on the side so that the nozzle can be moved beyond 25mm manually.

3.1.2 Fluid Flow Experimental Setup

A schematic of the fluid flow experimental setup can be seen in Figure 15. Two digital manometers were used to measure the pressure at the stagnation zone of the impinging jet. The whole range of nozzle-to-plate spacings needed to be measured with two manometers. The Meriam M200-DI0001 manometer has a range of 0-1 psi and an accuracy of ± 0.05% FS. The Meriam M200-DI0005 manometer has a range of 0-5 psi and an accuracy of ± 0.05% FS. At low nozzle-to-plate spacing, the jet produced a stagnation pressure value that was out of range of the 1 psi meter. The 5 psi meter was not sensitive enough to accurately measure the pressures at high nozzle-to-plate spacings.

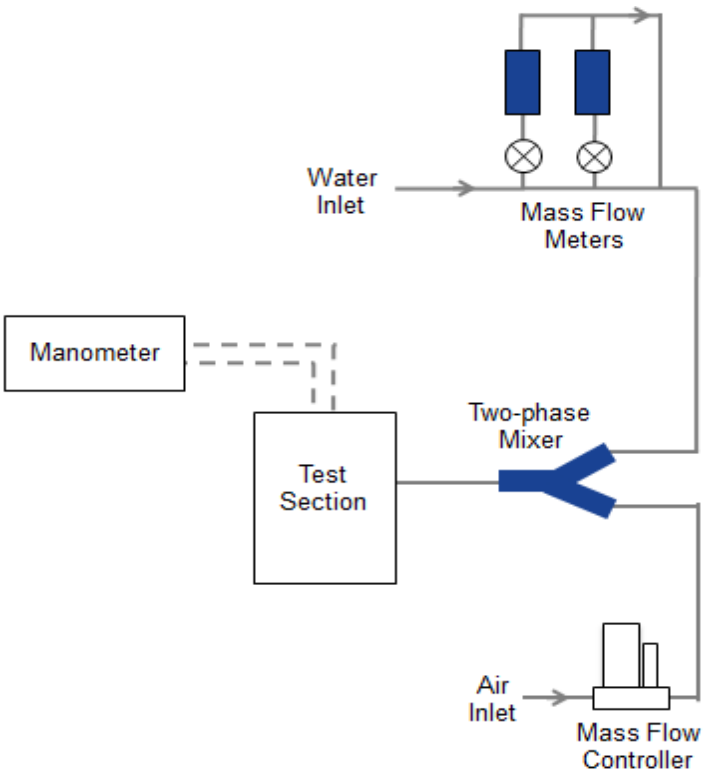

Figure 15: Schematic diagram of heat transfer experimental set-up [34].

The test section was made of transparent acrylic sheets that formed a box around the impingement surface as shown in Figure 16. The circular impingement surface was inside the test section, but elevated so that water could fall off of it and into the pool below. This was useful in the case of the free surface jet, because the water exiting the nozzle could flow off of the plate after it passed over the stagnation point without affecting the flow at the stagnation point. The impingement surface was a transparent acrylic sheet that was 5.5mm thick and 214mm in diameter. The stagnation point pressure was measured using a manometer, which was connected to an opening in the plate by flexible tubing. When the nozzle was mounted, it was centered directly above the opening that was

connected to the manometer. A cross sectional view of the fluid flow experimental setup can be seen in Figure 17.

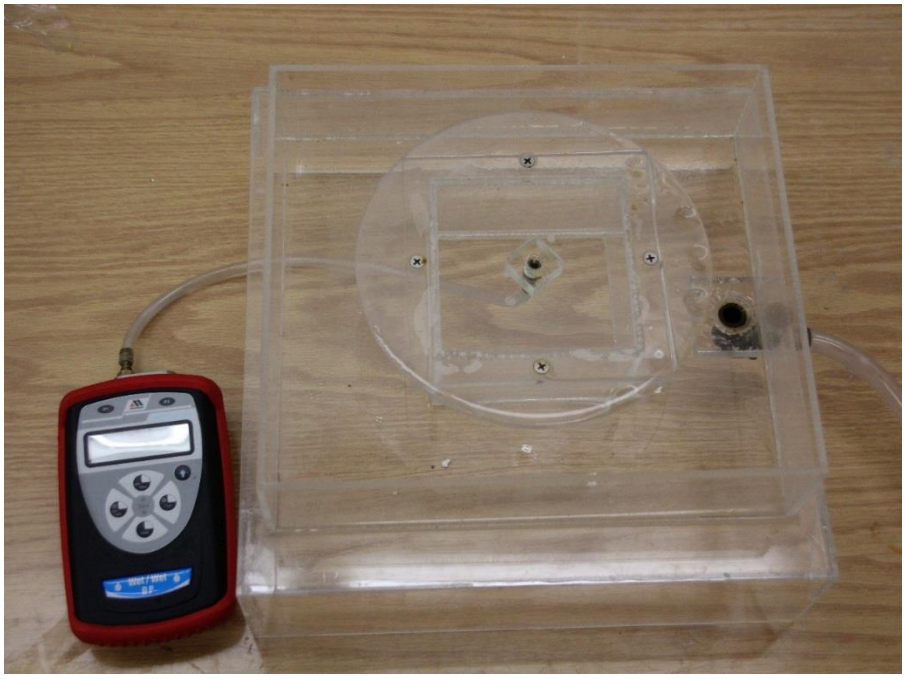

Figure 16: Test section for fluid flow experiment.

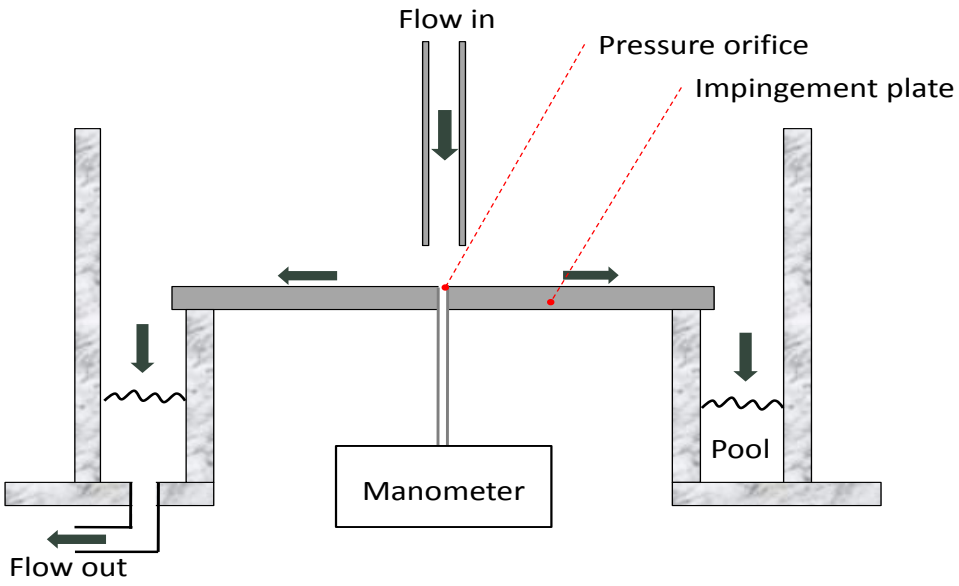

Figure 17: Cross sectional diagram of the fluid flow experimental setup [34].

The focus of this study is to compare the free surface jet and the submerged jet. For the submerged portion, the jet was submerged in a cylindrical tank that was 141.7mm in diameter and 43.2mm in height as shown in Figure 14. The setup of the fluid flow experiment can be seen in Figure 18.

Figure 18: Fluid flow experimental setup.

3.1.3 Heat Transfer Experimental Setup

The flow system and the cylindrical tank of the fluid flow experiment was used for the heat transfer experiment. A schematic of the heat transfer test section is shown in Figure 19.

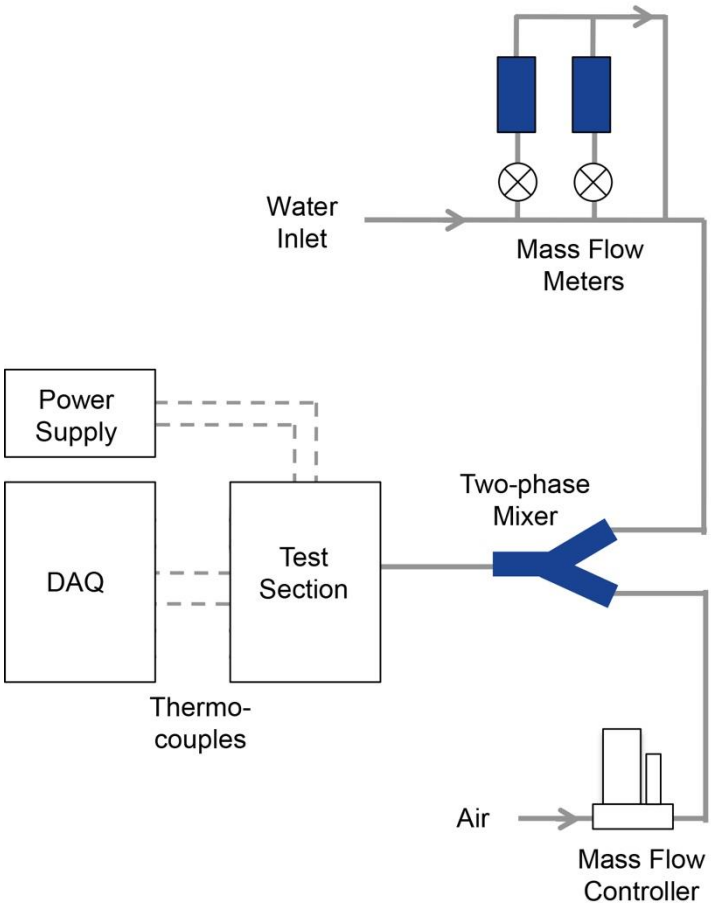

Figure 19: Schematic diagram of heat transfer experimental set-up [34].

The impingement surface was a disk made of PTFE Teflon. It was $20mm$ thick and $297mm$ in diameter. The Teflon disk was better suited as an impingement surface for the heat transfer experiment, because it provided insulation to minimize heat loss from the bottom of the heater. The heater was made of aluminum, ($0.01mm$ thick, $25mm$ wide and $44mm$ long). The test section of the heat transfer experiment was similar to that of the fluid flow experiment. The impingement surface and the test section can be seen in Figure 20.

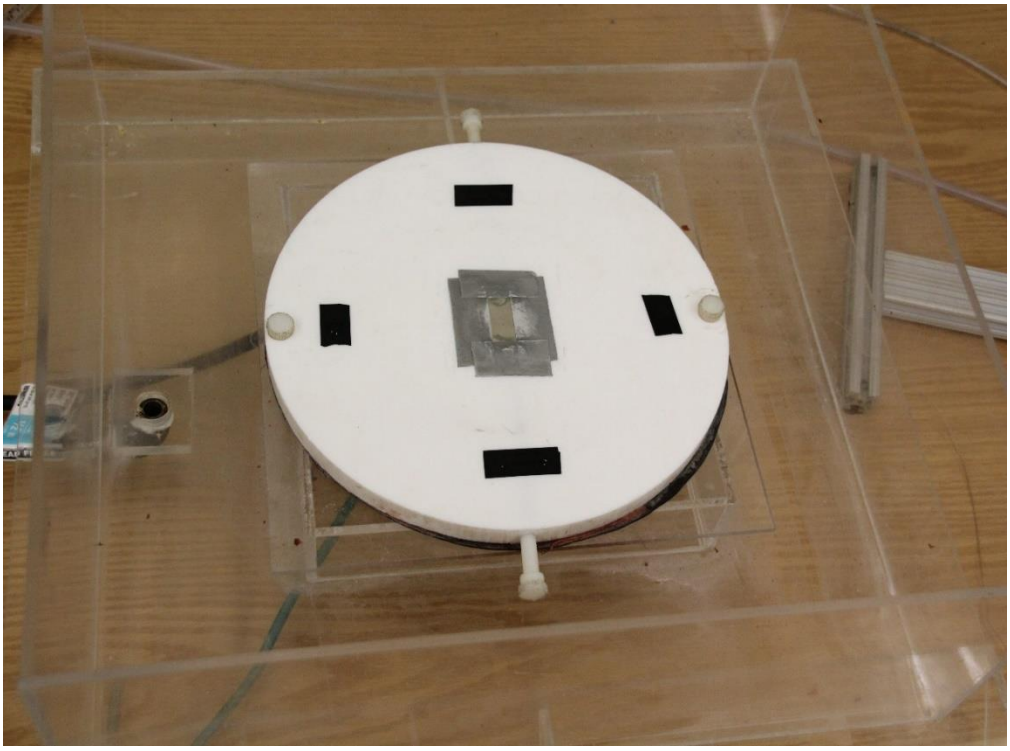

Figure 20: Impingement surface and the test section of heat transfer experimental setup.

The heater was mounted to the impingement surface by inserting the two ends into holes cut into the Teflon plate and then placing two copper bus bars. The holes were cut to fit the copper bus bars and the heater exactly. Once the heater was mounted, it was in contact with the copper bus bars. Along with the heater, a K-type thermocouple with a maximum service temperature of 260°C was also mounted to the impingement surface, then centered directly under the impinging jet. This was done by inserting it into a small hole drilled into the Teflon disk, and placed so that the tip of the thermocouple touched the heater. The thermocouple was mounted at the center of the heater. A second thermocouple was inserted 5 mm from the center of the jet.

Once the thermocouple was mounted, a strip of double sided tape was laid on top of the thermocouple, and covered the area under the heater. A hole was cut out of it, to allow the thermocouple to be in direct contact with the heater. The purpose of the double sided tape in between the heater and the Teflon impingement plate was to prevent water from flowing in between them. After the hole was cut, thermal paste (ThermalCoolFlux) with a thermal conductivity of $3.2\,\frac{W}{mK}$ was applied to the tip of the thermocouple. This was to eliminate air gaps and ensure maximum heat transfer.

The thermocouples were connected to an OMEGA OM-CP-QuadTemp2000 digital data acquisition system (DAQ). The DAQ was connected to a computer which recorded the temperature of the heater in real time. It can be seen in Figure 21. The copper bus bars, which were mounted onto the impingement surface to hold the heater in place, was connected to a DC power supply (Agilent 6651A #J03). This power supply allowed a nearly uniform heat flux boundary condition to be established at the plate. The impingement surface was attached to the test section using screws, and a heat resistant latex caulking (Nelson Latex Firestop Sealant) was used to seal any gaps between the Teflon disk and the acrylic test section. Although double sided tape was applied in between the heater and the Teflon impingement surface, it was noted that water could still be forced in between and affect the temperature of the thermocouple, especially during the submerged jet portion of the experiment. In order to eliminate the leaking, Duck Brand Waterproofing Tape was added around the edges of the heater. The setup of the heat transfer experiment can be seen in Figure 22. A cross sectional diagram of the heat transfer experimental setup can be seen in Figure 23.

Figure 21: Data acquisition unit.

Figure 22: Heat transfer overview of experimental test set-up.

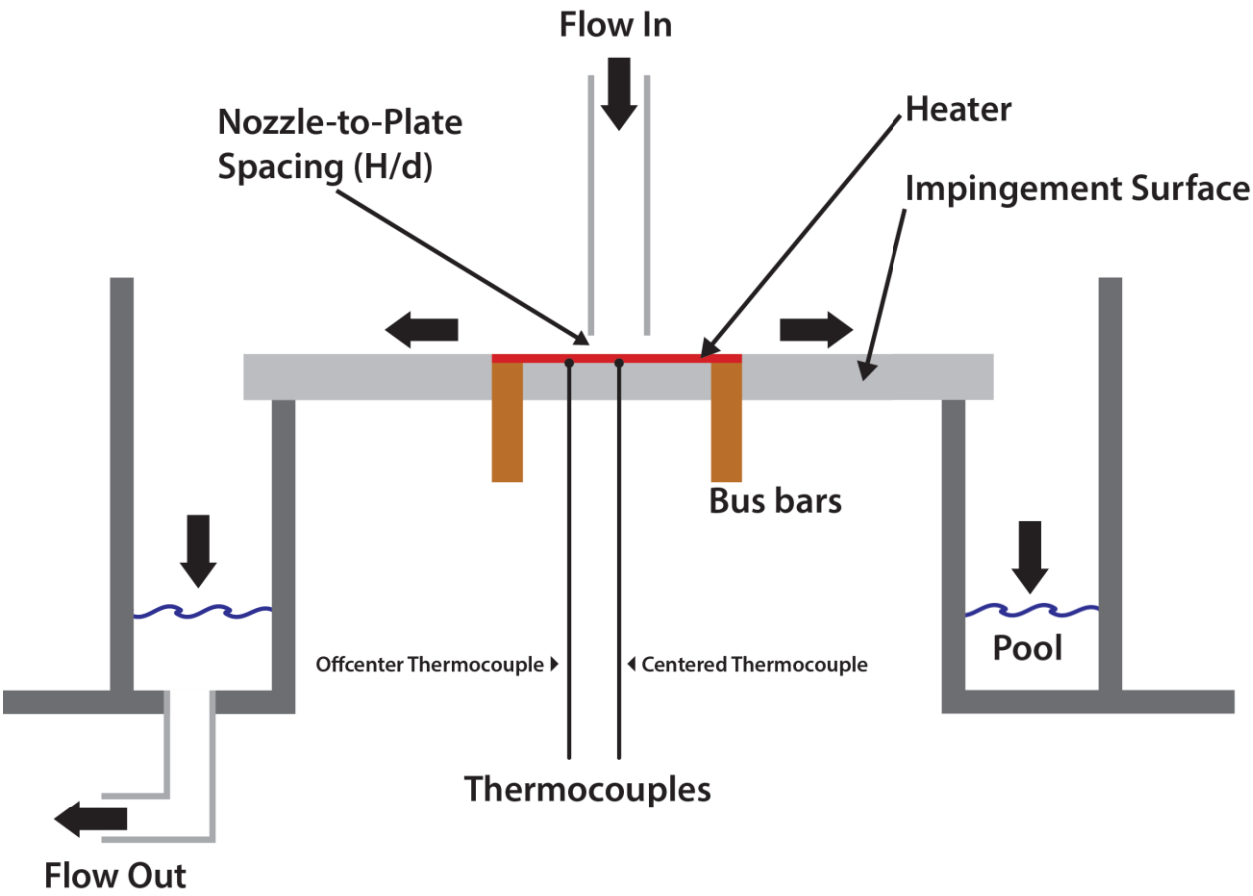

Figure 23: Cross sectional diagram of the heat transfer experimental set-up.

The setup needed to be switched between the submerged and free surface jet in between each nozzle-to-plate spacing without disturbing the nozzle-to-plate spacing, which was measured to 10 μm. To accomplish this, the tank was a cylinder with no top or bottom so it could be set on the impingement plate to achieve a submerged jet, or lifted up in order to achieve a free surface jet. A metal rod was used to lift the tank during the free surface jet portion of the experiment, and can be seen in Figure 24. A rubber gasket of the same diameter was placed in between the tank and the plate so that the water would fill the tank instead of spilling out of the bottom.

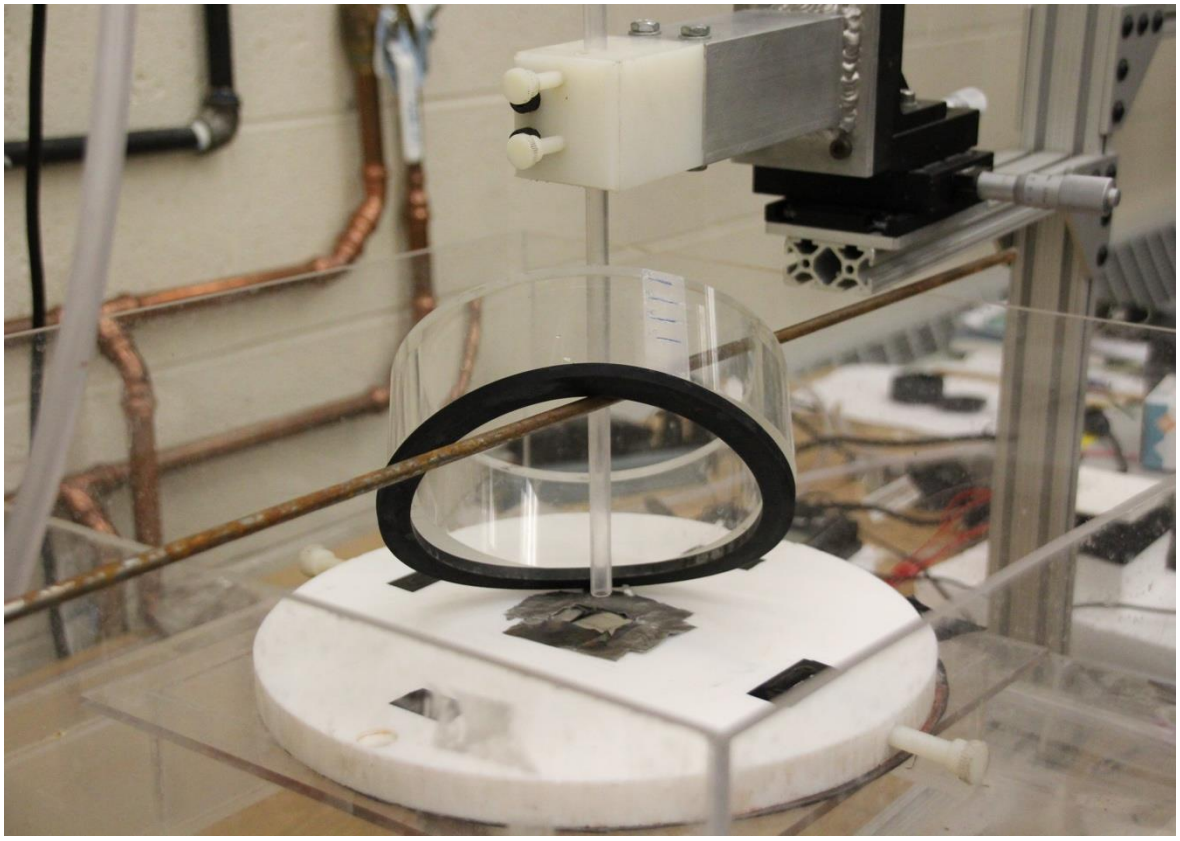

Figure 24: Metal rod used to lift the tank during the free surface jet portion of the experiment

3.2 Procedure

During the fluid flow experiment, the pressure of the jet at the stagnation point was taken at multiple nozzle-to-plate spacings, ranging from $0.2mm < H < 50mm$. Pressure was measured with the 1psi and 5psi manometer.

The fluid flow data was taken by placing the impinging jet directly in line with the orifice connected to the manometer. For each volumetric quality, the correct volumetric flow rate of air was chosen for a constant volumetric flow rate of water ($1.4721 \times$

10^{-5} $\frac{m^3}{s}$). The pressure measurement was taken at 25 nozzle-to-plate spacings ranging from $0.03 < H/d < 8.5$ at a volumetric quality, and then the volumetric quality was changed.

The pressure measurements were not recorded in real time, so each data point was taken by approximating the value of the fluctuating pressure readings given by the manometer. The manometer also had a max/min feature. By resetting the max/min at every nozzle-to-plate spacing, the full range of pressures was attained. Before recording the maximum and minimum value, the jet impinged on the surface for at least five seconds, to allow the full range to be recorded. The average of the maximum and minimum was calculated and compared to the approximated value.

The heat transfer portion of the experiment was similar to the fluid flow portion. The nozzle, which was mounted on the stage, was centered directly over the thermocouple. Before data could be recorded for the heat transfer test, the temperature of the jet at the exit of the nozzle was needed. This temperature was determined by starting the jet with the lowest nozzle-to-plate spacing ($H/d = 0.03$) and recording the temperature reading of the thermocouple. This value served as T_∞. This value was obtained for every volumetric quality, before the start of the experiment. Once this value was recorded, the voltage could be applied to the heater. Using the DC power supply, the voltage was set to 5V and the current was set to 50.707A. A data point could be taken once the temperature reached steady-state.

The temperature data was taken for the free surface jet and the submerged jet using two methods. In the first method, the tank was set up around the nozzle so that the jet was

submerged. At each nozzle-to-plate spacing, the temperature of the submerged jet was recorded, then the tank was lifted up using the metal rod and the temperature of the free surface jet was recorded. Approximately two to three minutes elapsed in between each nozzle-to-plate spacing, depending on how long it took for each to reach steady-state. Once steady-state was reached, the temperature was recorded. This method served as the comparison between the free surface jet and the submerged jet. In the second method, the free surface jet data and the submerged jet data were taken separately. The temperature for each nozzle-to-plate spacing was taken for the full range of the free surface jet and then the experiment was reset and the entire range of temperatures were taken for the submerged jet. This method served as the comparison between the trends of the stagnation pressure and Nusselt number trends in each region.

Uncertainty analysis was conducted on each individual measured value. The individual values and total uncertainty can be seen in Table 2.

Table 2: Uncertainty analysis.

Individual Measured Value		$\left\|\frac{\delta x_i}{Nu}\frac{\partial Nu}{\partial x_i}\right\|\times 100(\%)$
x_i	Unit	
T_i	℃	1.57
T_{in}	℃	2.01
I	A	0.89
V	V	1.80
q_{loss}	W	0.84
d_h	m	0.34
A	m^2	2.36
k	W/mK	0.08
Total uncertainty: $\delta Nu/Nu = 4.11\%$		

CHAPTER 4

RESULTS AND DISCUSSION

4.1 Stagnation Pressure and Nozzle-to-plate Spacing

The stagnation pressure was obtained by taking an approximated value and the average of the maximum and minimum value. For $\beta = 0.1$, the approximated and average values are within 5% for the submerged jet values, and 10% for the free surface jet values. For $0.3 < \beta < 0.7$, the variation between the two values were within 15%. For $\beta = 0.9$, the two values were within 37% for the submerged jet and 54% for a free surface jet. This is due to the increase in pressure fluctuation at $\beta = 0.9$.

The approximated value was chosen to show the relationship between stagnation pressure and nozzle-to-plate spacing. The variation of the stagnation pressure as a function of normalized nozzle-to-plate spacing for both free surface and submerged jet can be seen in Figures 25 and 26. The results of the pressure values were divided into three regions. Region I ranges from $0 < H/d < 1.2$, Region II ranges from $1.2 < H/d < 3$. Region III ranges from $3 < H/d < 8.5$.

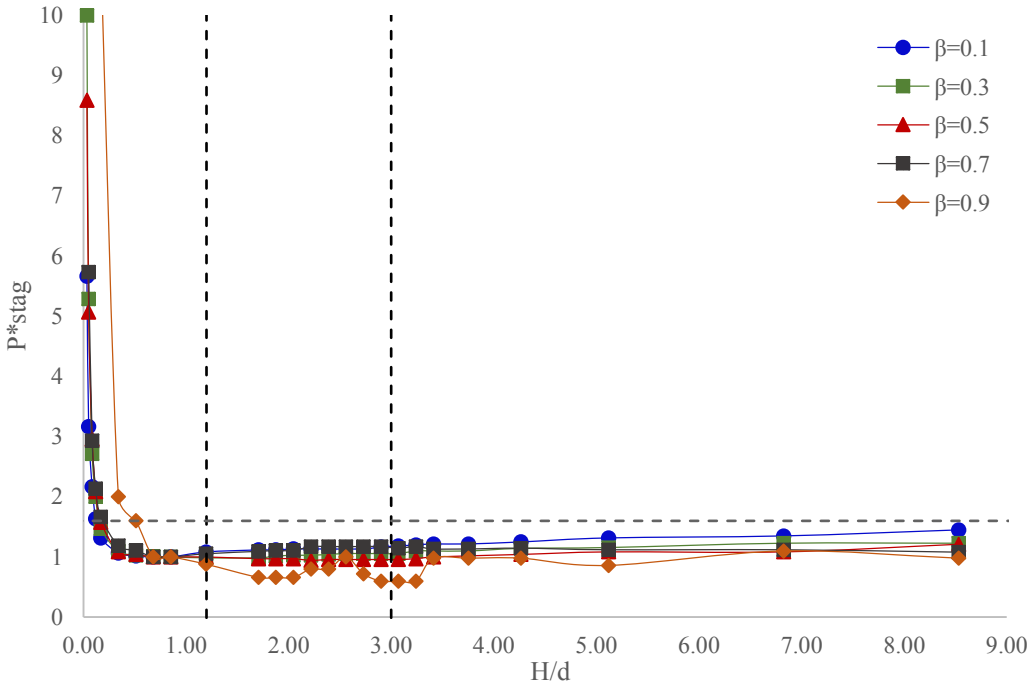

Figure 25: Normalized stagnation pressure as a function of normalized nozzle-to-plate spacing for a free surface jet at 5 volumetric qualities.

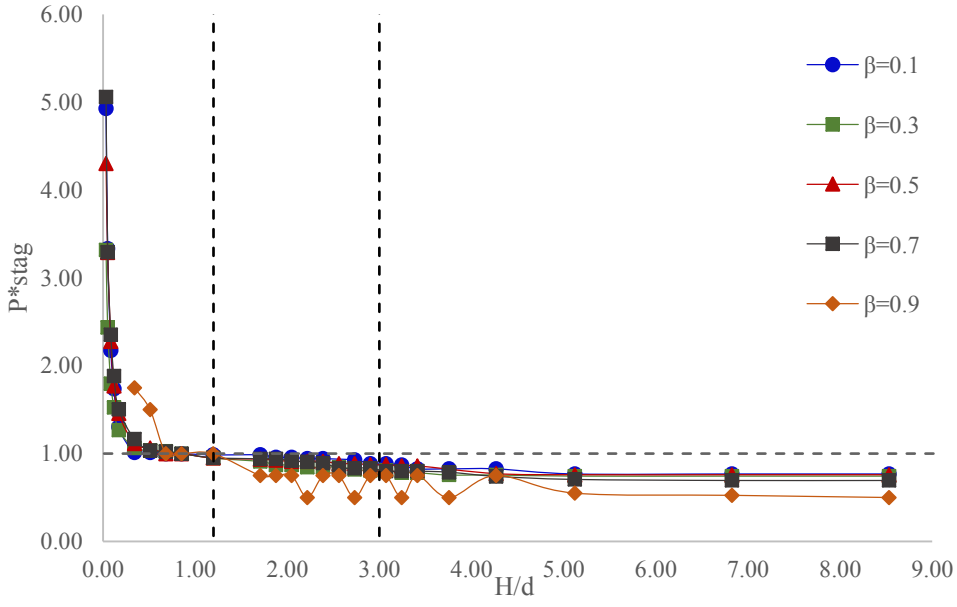

Figure 26: Normalized stagnation pressure as a function of normalized nozzle-to-plate spacing for a submerged jet at 5 volumetric qualities.

As shown in Figure 25, the free surface and submerged jet experienced an exponential decrease in the stagnation pressure as a function of nozzle-to-plate spacing in Region I, $0 < H/d < 1.2$. In this region, the pressure is governed by the extended Bernoulli's equation:

$$P_0 = \frac{1}{2}\rho u_1^2 + \frac{K}{2}\rho u_2^2 \tag{8}$$

where the stagnation pressure included the effect of the dynamic pressure from u_1 and the jet deflection effect from u_2 as shown in Figure 27. *K* is the jet deflection coefficient, and is obtained empirically from Figures 25 and 26.

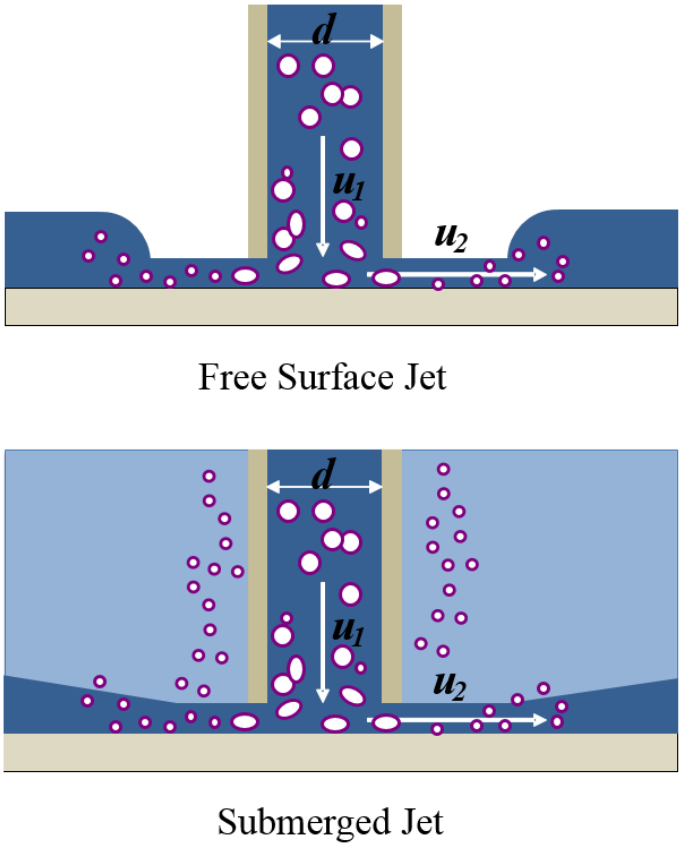

Figure 27: Dynamic pressure and jet deflection effect of free surface and submerged jet at low nozzle-to-plate spacing.

Region I, $0 < H/d < 1.2$ of the submerged jet forms the stagnation region, or jet deflection region, where the pressure increased rapidly as it approached the plate. Recall that the length of the stagnation region according to the value obtained by Schrader is approximately 1.2 nozzle diameters. Within this length, the flow is influenced by the impingement surface. In Region I, the pressure decreased exponentially as the nozzle-to-plate spacing increased. In this region, the nozzle exit was within the stagnation region of the jet, where the impingement surface caused a large increase in pressure, and the jet does not behave as a free submerged jet. Turbulence due to mixing begins to develop, but at this

height, it is not completely developed. The axial velocity of the jet is decreasing and the radial velocity of the jet is increasing in this region.

In Region II and III, $1.2 < H/d < 8.5$ of the free surface jet, the stagnation pressure increased linearly. For $0.1 < \beta < 0.7$, the free surface jet reached its minimum pressure value near $H/d = 0.5$, and increased linearly with increasing nozzle-to-plate spacing. For $\beta = 0.9$ the stagnation pressure values fluctuated and did not increase as the other volumetric qualities. The linear increase can be attributed to the acceleration due to gravity, which has the largest effect on the lower volumetric qualities. The volumetric quality $\beta = 0.9$ consists of mostly air. Therefore gravity affects it the least, and it increased the least with increasing nozzle-to-plate spacing. The trend of the stagnation pressure is governed by Bernoulli's equation:

$$P_0 = \frac{1}{2}\rho u_1^2 + \rho g H \tag{9}$$

where H is the distance between the nozzle and the plate. As the nozzle-to-plate spacing increased, the stagnation pressure increased. This can be seen in Figure 28.

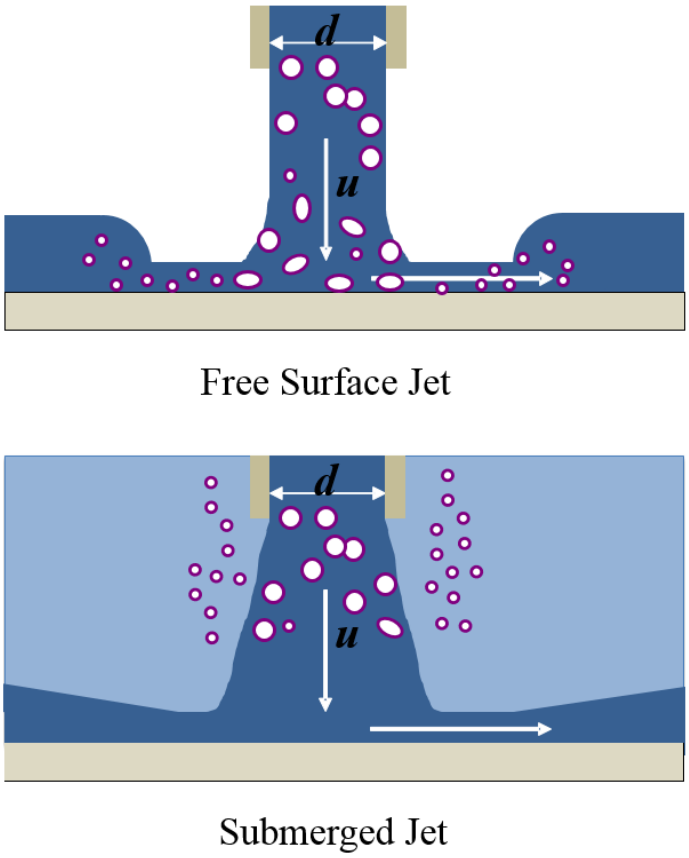

Figure 28: Stagnation pressure of free surface and submerged jet at high nozzle-to-plate spacing.

In Region II and III, $1.2 < H/d < 8.5$ the stagnation pressure of the submerged jet decreased linearly as the nozzle-to-plate spacing increased. As the nozzle-to-plate spacing increased, the effect of the jet itself on the stagnation pressure decreased. Because the jet was submerged in water, the jet must overcome the force of the water that separates it from the impingement surface. Thus, the stagnation pressure is determined by the dynamic pressure term and a flow resistance term:

$$P_0 = \frac{1}{2}\rho u_1^2 + \psi \tag{10}$$

where ψ is the flow resistance. As seen in Figures 29 - 35. It is likely that the pressure value would continue to decrease and approach the value of the pressure caused by the weight of the water in the tank as the nozzle-to-plate spacing increased beyond the data shown in Figure 26.

Figure 29: Submerged jet at $\beta = 0.9$ and $H/d = 0.03$. At the lowest nozzle-to-plate spacing, the jet touches on the impingement surface.

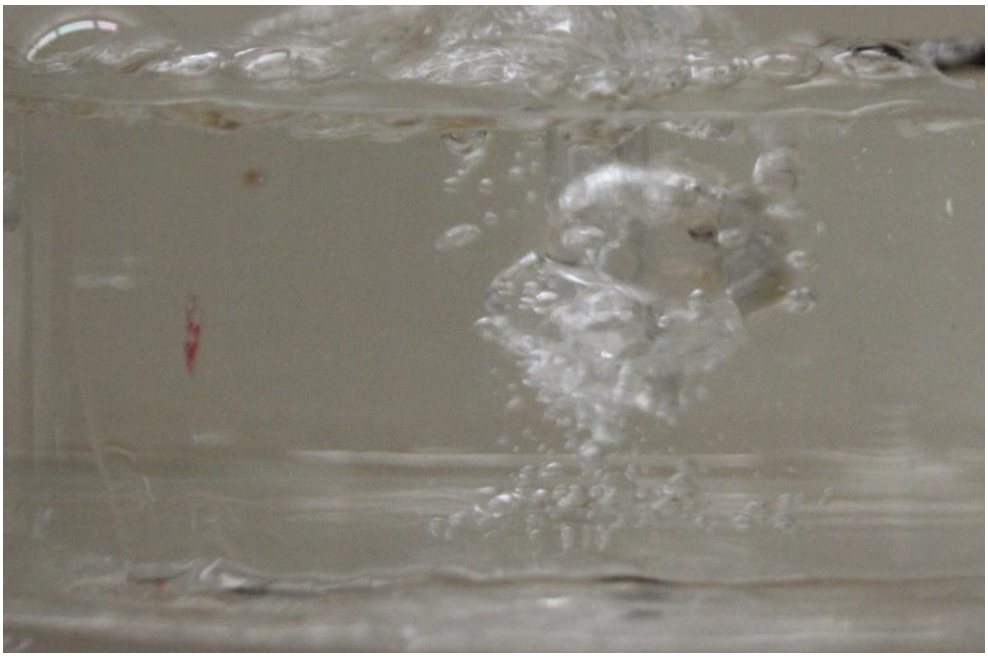

Figure 30: Submerged jet at β = 0.9 and H/d = 4.27, a clear separation has formed between the jet and the impingement surface during a fluctuation.

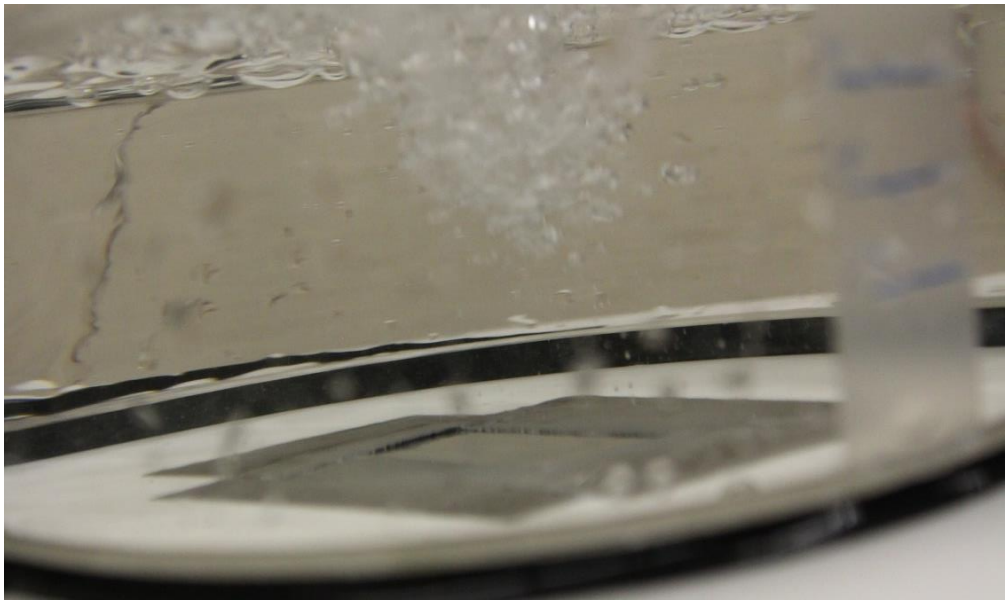

Figure 31: Submerged jet at β = 0.9 and H/d = 8.53, there is a clear separation between the jet and the impingement surface.

As shown in Figures 29 - 31 for $\beta = 0.9$, the bubbles touch the impingement surface at $H/d = 0.03$. At $H/d = 4.27$, a gap becomes visible, although since the pressure is fluctuating, it is not visible at all times. At $H/d = 8.53$, the separation between the bubbles and the impingement surface becomes apparent during pressure fluctuations. At this nozzle-to-plate spacing, the bubbles and the jet itself are not the dominant factor of the pressure. The pressure approaches the value of weight of the water in the tank.

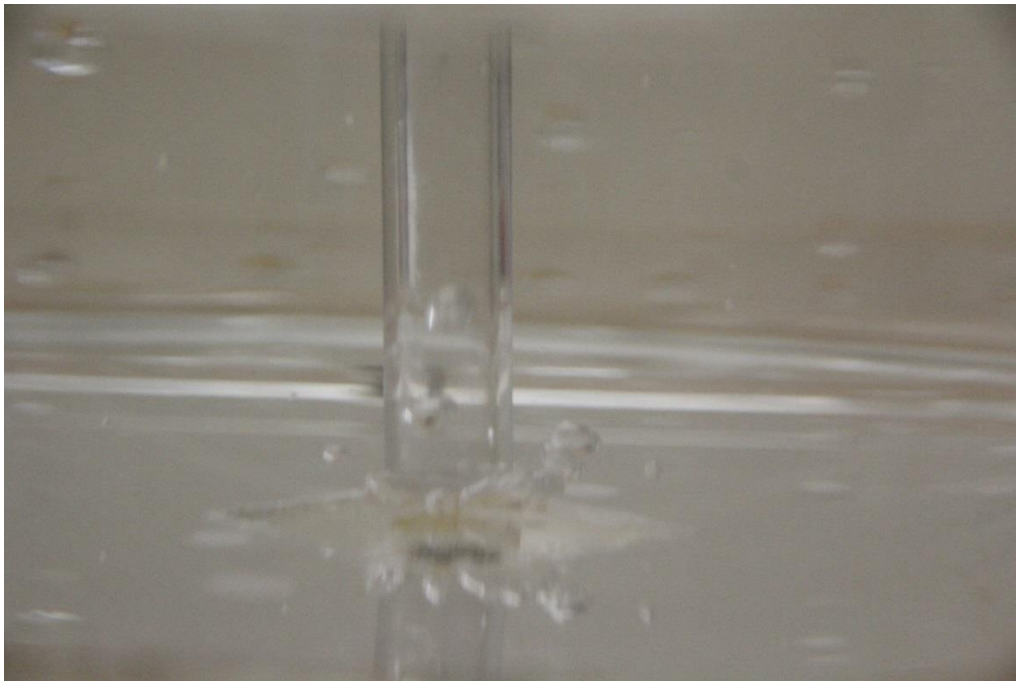

Figure 32: Submerged jet at β = 0.1 and H/d = 0.03. At the lowest nozzle-to-plate spacing, the jet touches on the impingement surface.

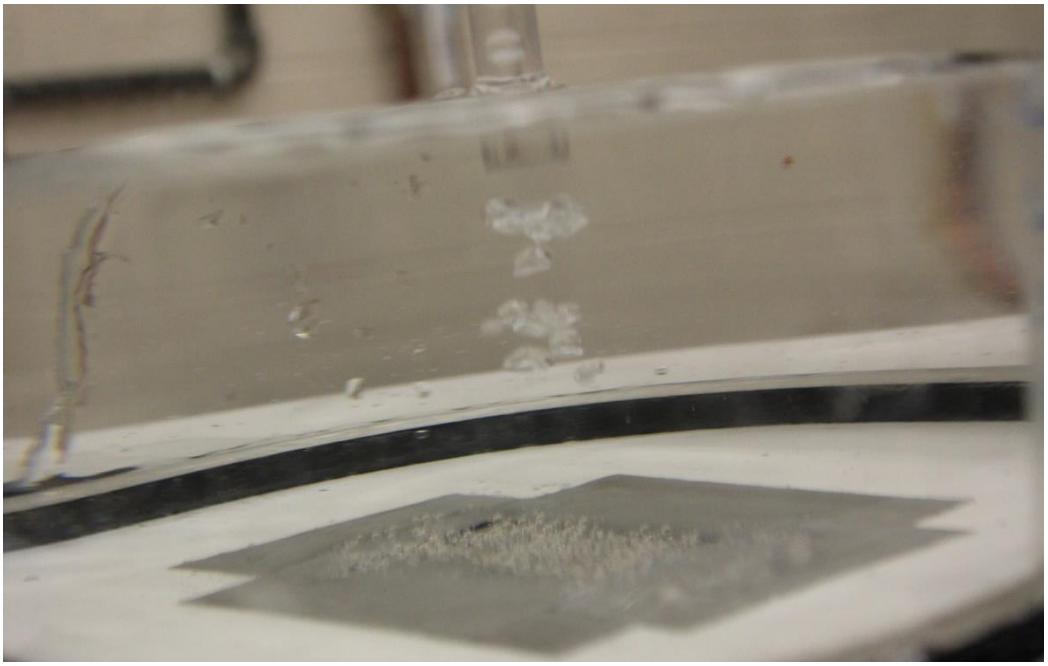

Figure 33: Submerged jet at β = 0.1 and H/d = 8.53, there is a clear separation between the jet and the impingement surface.

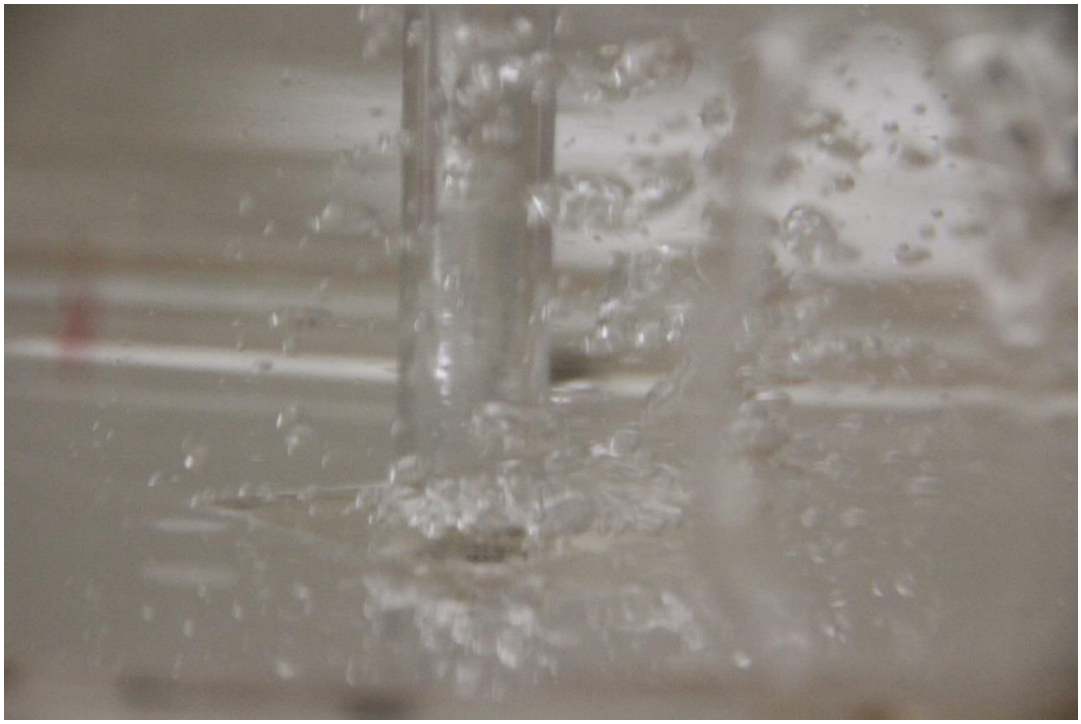

Figure 34: Submerged jet at β = 0.3 and H/d = 0.03. At the lowest nozzle-to-plate spacing, the jet touches on the impingement surface.

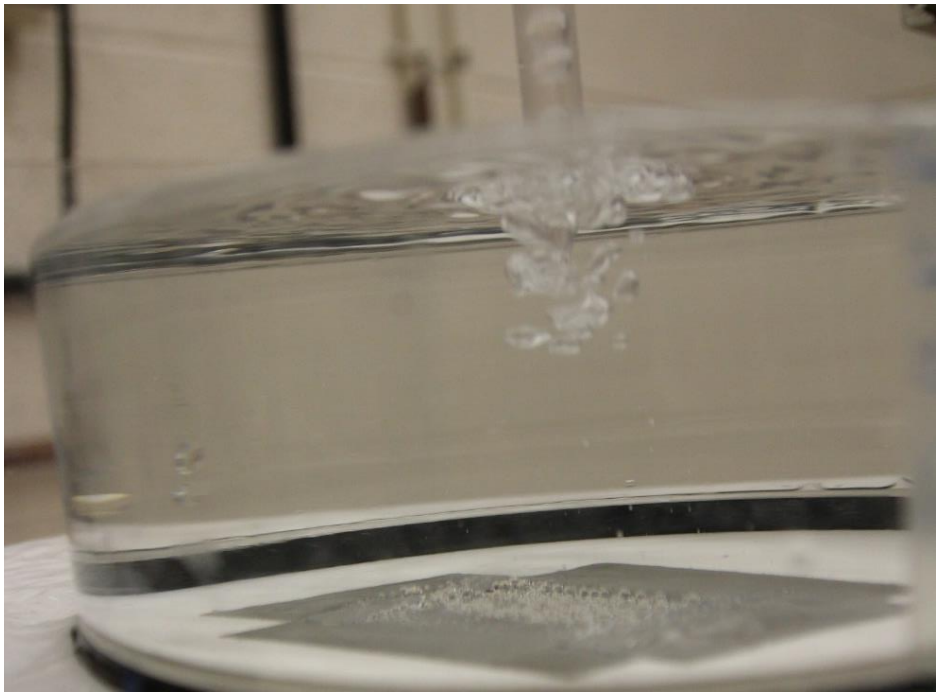

Figure 35: Submerged jet at β = 0.3 and H/d = 8.53, there is a clear separation between the jet and the impingement surface.

Figures 32 - 35 show the difference between $H/d = 0.03$ and $H/d = 8.53$ at $\beta = 0.1$ *and* 0.3. The bubbles touch the impingement surface at $H/d = 0.03$. At $H/d = 8.53$, the separation between the bubbles and the impingement surface becomes apparent. This separation between the jet and the impingement surface affects not only the stagnation pressure, but the Nusselt number as well.

4.2 Fluctuation and Nozzle-to-Plate Spacing

The variation of the pressure fluctuation with nozzle-to-plate spacing can be seen in Figures 36 and 37. The results of the pressure values are divided into two regions. Region I ranges from $0 < H/d < 1.2$, and Region II ranges from $1.2 < H/d < 8.5$. The pressure fluctuation trends are similar to the trends of the pressure.

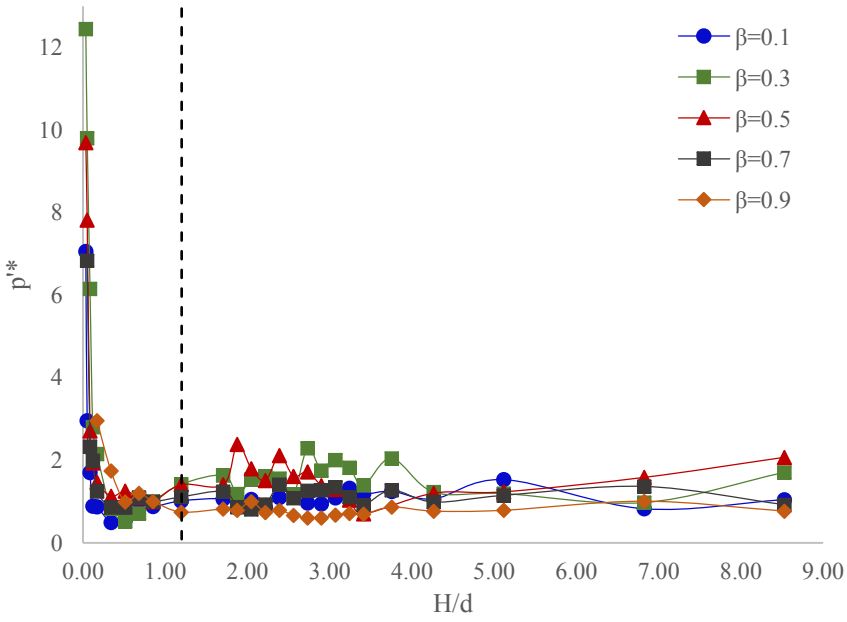

Figure 36: Variation of pressure fluctuation with nozzle-to-plate spacing for the free surface jet at 5 volumetric qualities.

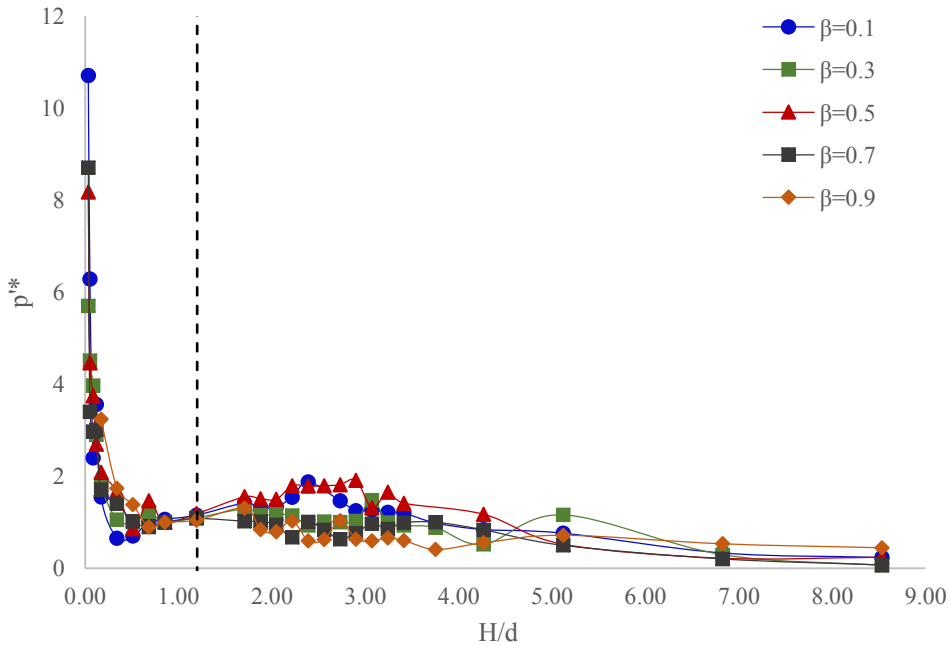

Figure 37: Variation of pressure fluctuation with nozzle-to-plate spacing for the submerged jet at 5 volumetric qualities.

Both jets experienced an exponential decrease in the stagnation region as the nozzle-to-plate spacing increased in Region I, $0 < H/d < 1.2$. In Region II, $1.2 < H/d < 8.5$ the stagnation pressure increased linearly in the free surface jet and decreased linearly in the submerged jet. There is still much to be understood about the pressure fluctuation of impinging jets, especially those with two-phase flow.

4.3 Nusselt Number

The temperature data of the heat transfer experimental setup was taken using two methods. In the first method, the data for the free surface jet and submerged jet were taken by alternating between the two in between each nozzle-to-plate spacing. In the second

method, the data for the full range of each was taken separately. The data of the first method showed the comparison between the Nusselt number of the submerged and free surface jet. During each alternation, the temperature would either drop or rise when switching from submerged to free surface jet. However, switching between the two may have affected the trends of each. The trends obtained in this method fluctuated and varied greatly between trials. It was noted that the higher or lower temperature from the submerged jet may have affected the temperature reading from the free surface jet and likewise, the free surface jet temperature may have affected the submerged jet temperature, even though the system was allowed to reach steady state. The data of the second method showed the comparison between the stagnation pressure and Nusselt number trends in each region. When taken separately however, it is not accurate to compare the values of the Nusselt number between the free surface jet and the submerged jet due to fluctuations in water temperature and voltage that may occur between trials. Therefore both methods were used. The results of each can be seen in the following sections. The results given by the alternating method yielded a precise comparison between the two jets, but not a precise trend. The given by taking the data separately yielded more precise trend results, but not a precise comparison between the two jets.

4.3.1 Nusselt Number and Nozzle-to-plate Spacing

The variation of the Nusselt number of each normalized nozzle-to-plate spacing can be seen in Figures 38 and 39. Analyses of the results can be divided into three regions. Region I ranges from $0 < H/d < 1.2$, Region II ranges from $1.2 < H/d < 3$. Region III ranges from $3 < H/d < 8.5$.

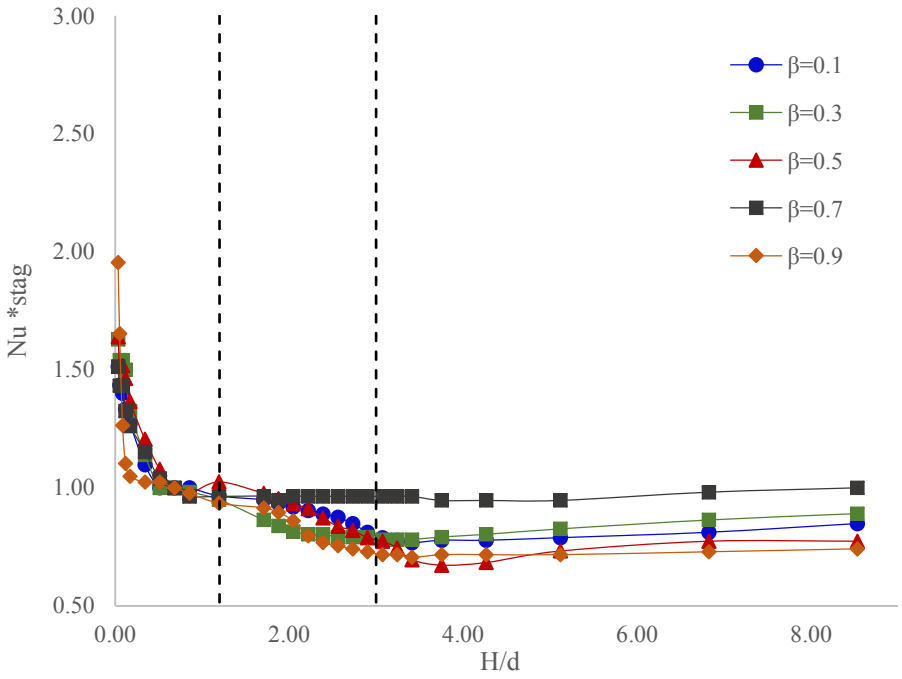

Figure 38: Stagnation Nusselt number as a function of dimensionless H/d for a free surface jet at 5 volumetric qualities.

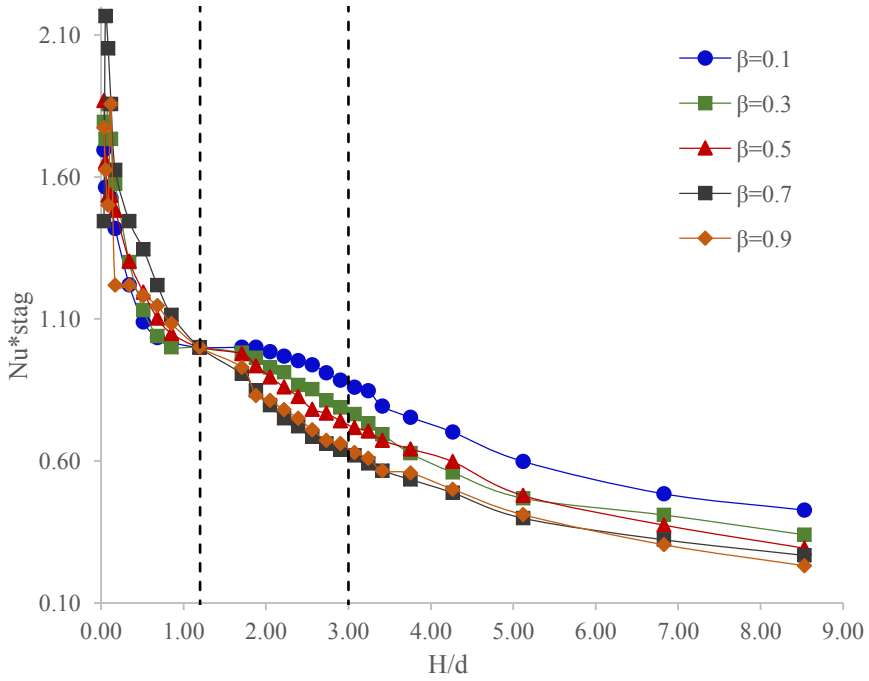

Figure 39: Stagnation Nusselt number as a function of dimensionless H/d for a submerged jet at 5 volumetric qualities.

In Region I, $0 < H/d < 1.2$, the Nusselt number decreased exponentially as the nozzle-to-plate spacing increased for both the free surface jet and the submerged jet. This trend corresponds to the trend of the stagnation pressure values from $0 < H/d < 1.2$. The Nusselt number reached a minimum value at $H/d \approx 0.85$, and remained constant with some fluctuation as the flow exits the stagnation region and approaches Region II. Based on the results of the pressure measurements, it is expected that the Nusselt number is highest at low nozzle-to-plate spacings. Here the jet has the highest stagnation pressure and velocity. For the submerged jet, this exponential decrease is within the stagnation region.

In Region II, $1.2 < H/d < 3$ the Nusselt number of the free surface jet decreased linearly as it approached Region III for all volumetric qualities except $\beta = 0.7$ which remained constant. In Region II of the submerged jet, the Nusselt number decreased linearly for all volumetric qualities.

In Region III, the trend of the trends differed between submerged and free surface jets. The Nusselt number of the free surface jets for all volumetric qualities increased linearly. This can be attributed to the increase in stagnation pressure. The Nusselt number of the submerged jets decreased linearly for all volumetric qualities. As the nozzle-to-plate spacing increased, the jet had a larger distance to travel to reach the plate. Because the jet was submerged, the jet must be forced through the water that separates it from the impingement surface.

4.3.2 Nusselt Number and Stagnation Pressure

The Nusselt number and stagnation pressure trends were similar for each volumetric quality. It has been shown in previous research that the Nusselt number can be expressed as a function of stagnation pressure only in free surface jets. Friedrich [34] showed this when studying the effect of volumetric quality on the Nusselt number of free surface impinging jets. Therefore, the results have been divided into each volumetric quality for both free surface and submerged jets, and they can be seen in Figures 40 - 49. The results can be broken into three regions. Region I ranges from $0 < H/d < 1.2$, Region II ranges from $1.2 < H/d < 3$. Region III ranges from $3 < H/d < 8.5$.

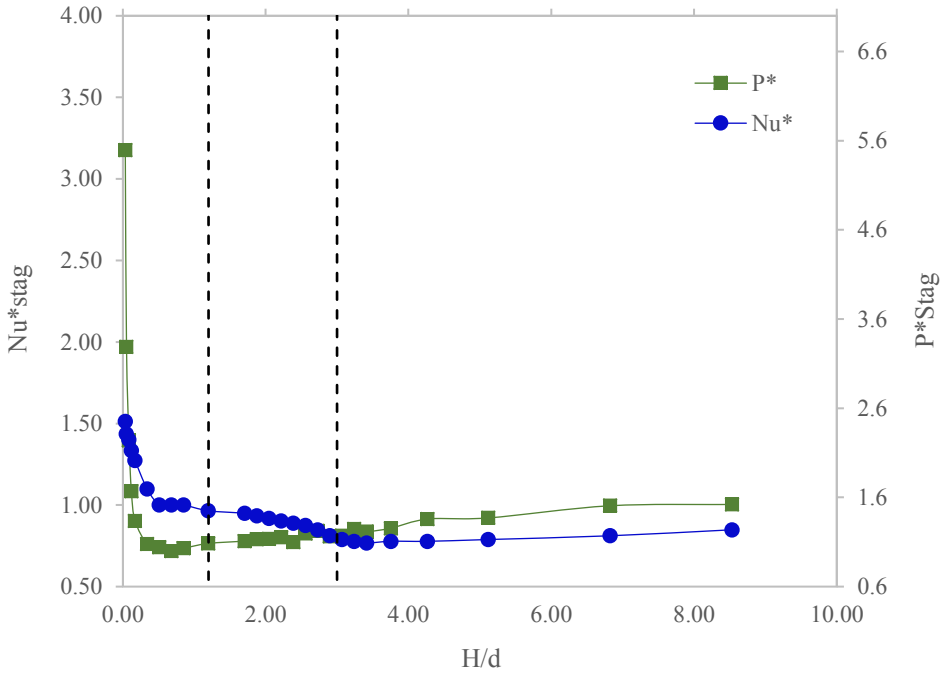

Figure 40: Nusselt number and stagnation pressure trends for β = 0.1 in the free surface jet.

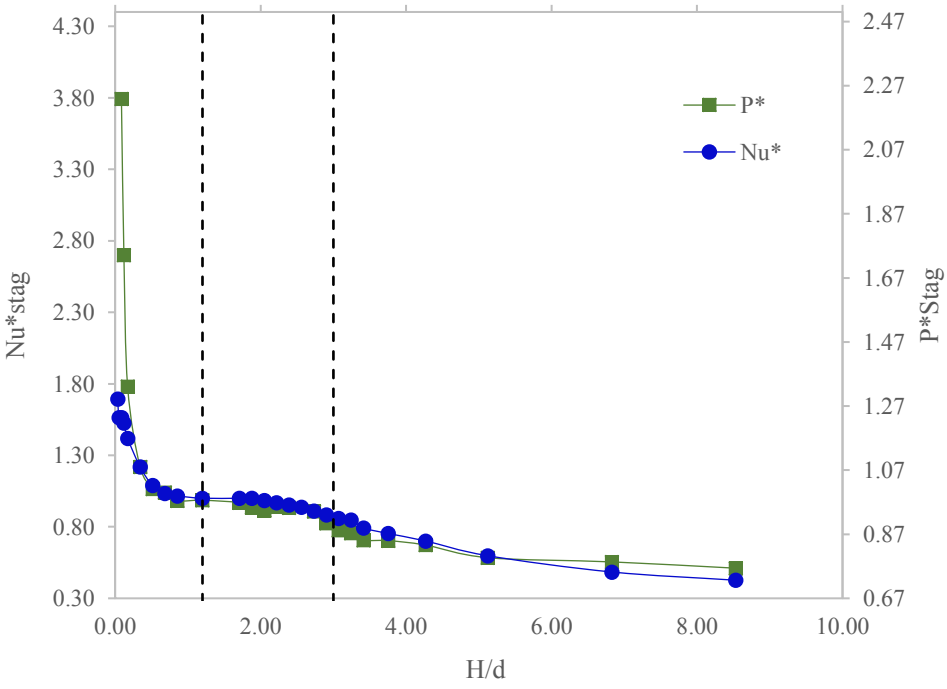

Figure 41: Nusselt number and stagnation pressure trends for β = 0.1 in the submerged jet.

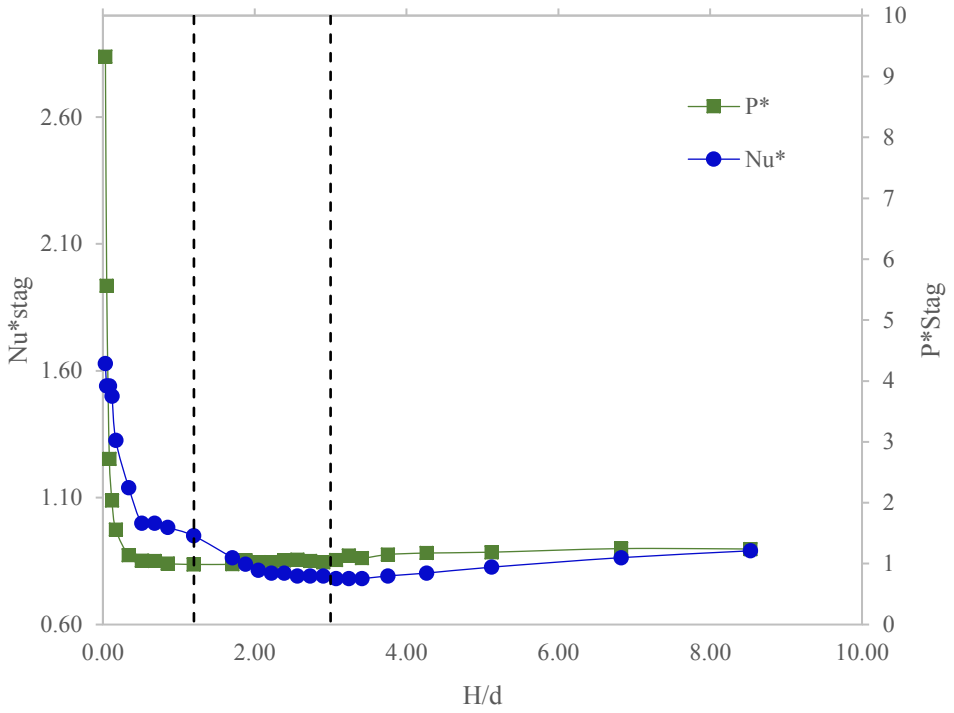

Figure 42: Nusselt number and stagnation pressure trends for β = 0.3 in the free surface jet.

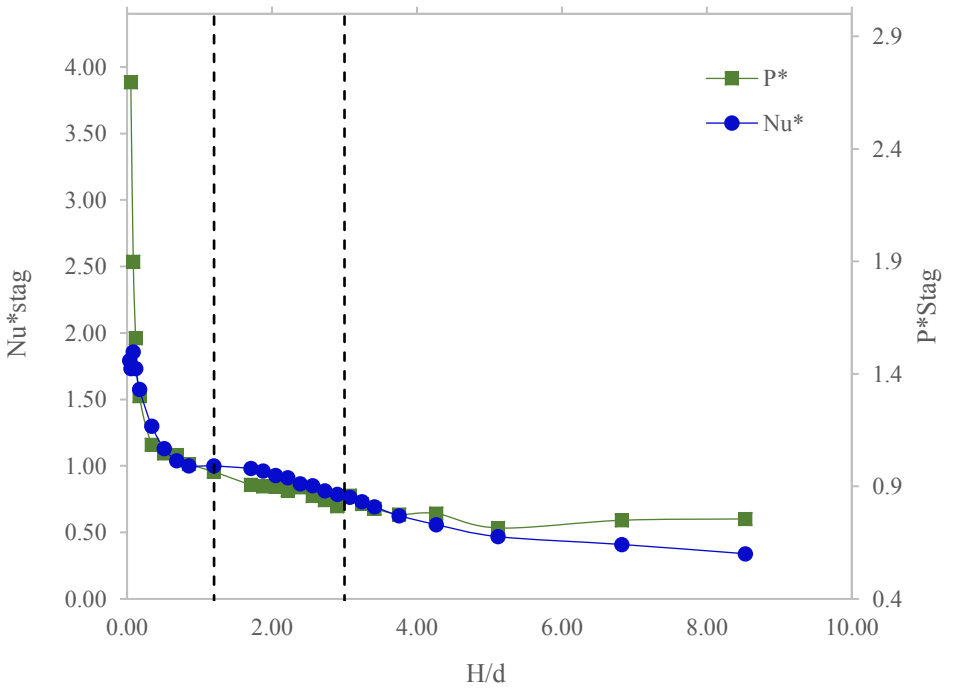

Figure 43: Nusselt number and stagnation pressure trends for β = 0.3 in the submerged jet.

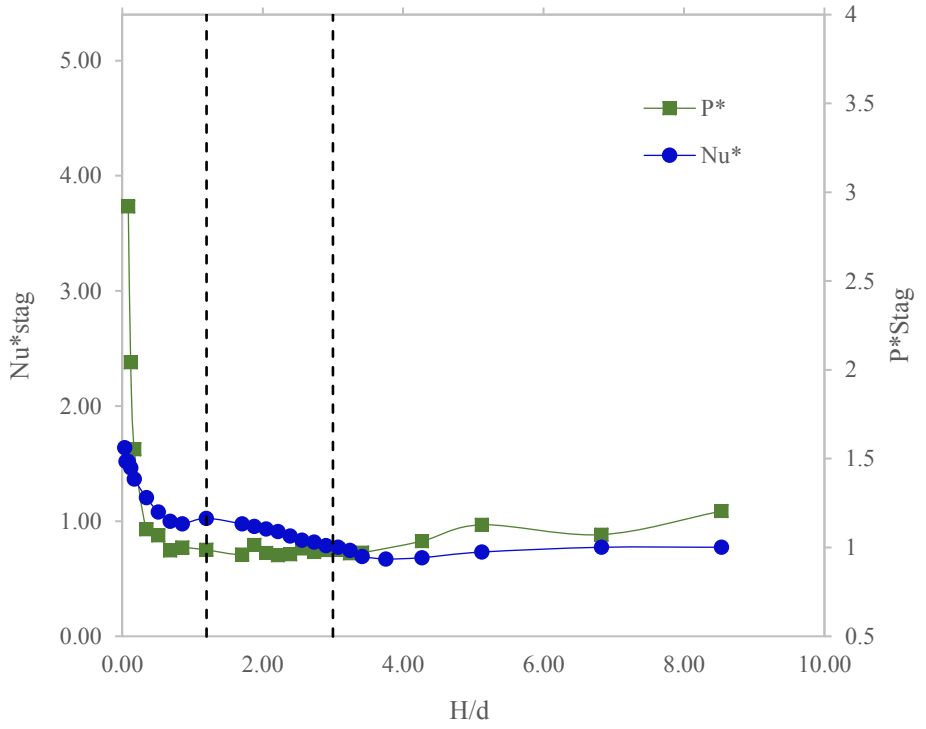

Figure 44: Nusselt number and stagnation pressure trends for β = 0.5 in the free surface jet.

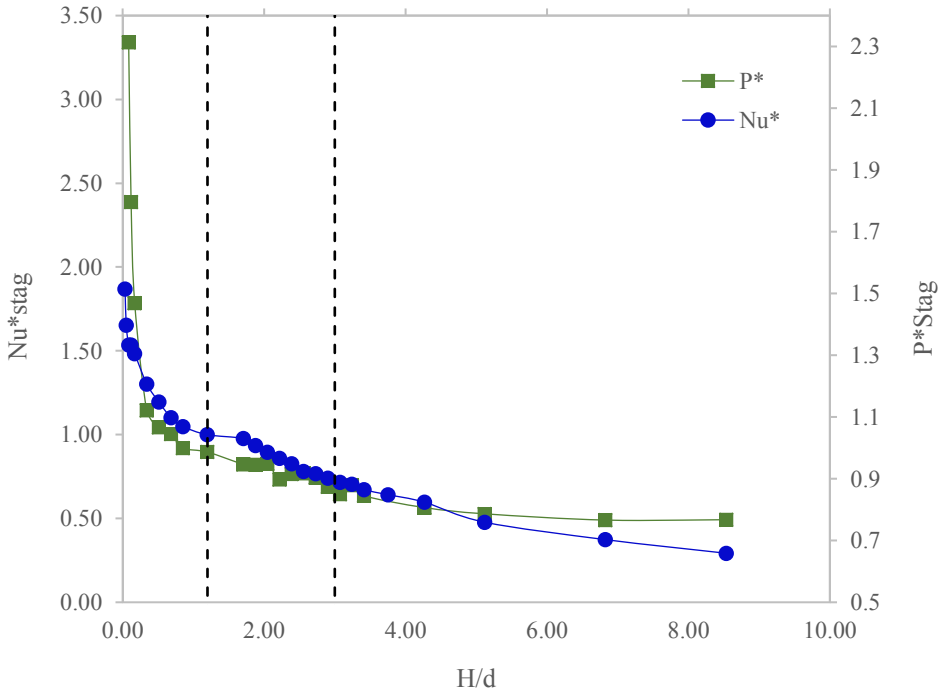

Figure 45: Nusselt number and stagnation pressure trends for β = 0.5 in the submerged jet.

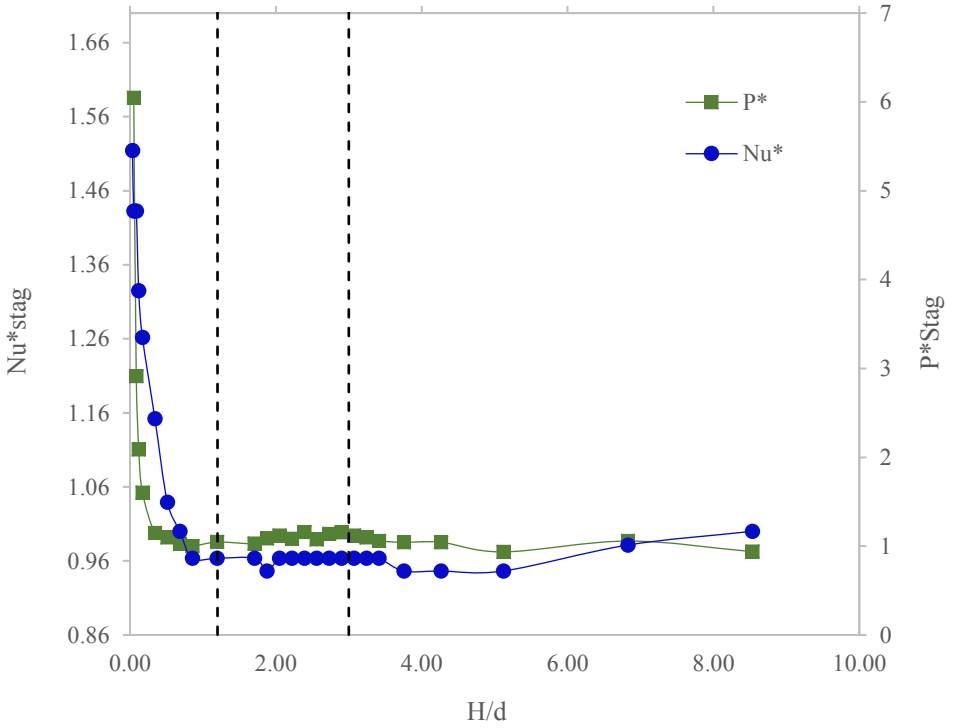

Figure 46: Nusselt number and stagnation pressure trends for β = 0.7 in the free surface jet.

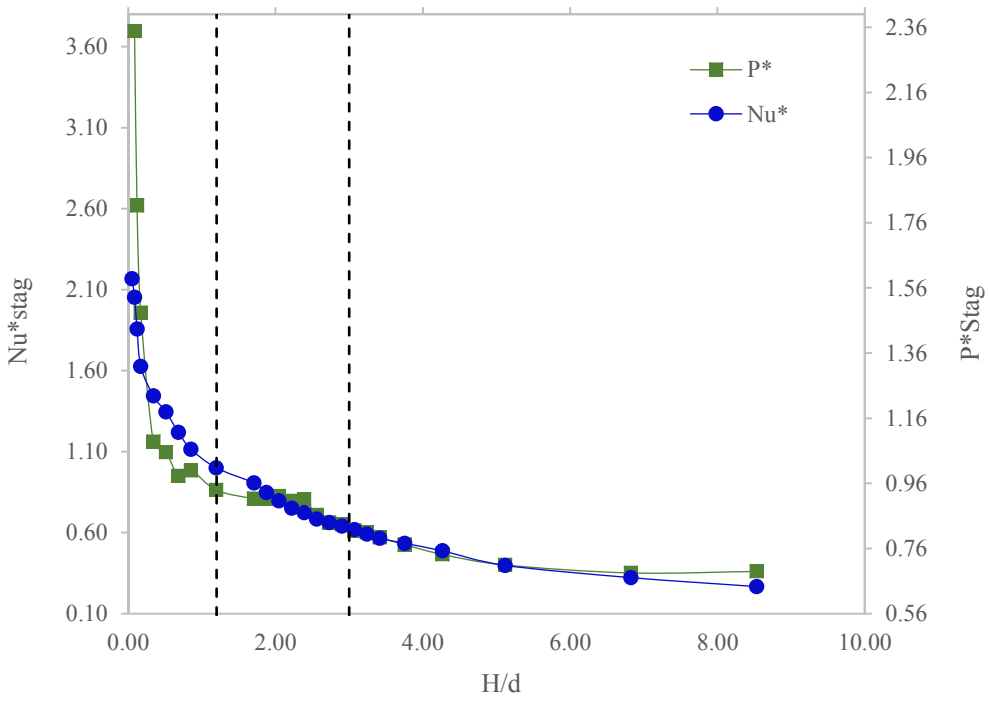

Figure 47: Nusselt number and stagnation pressure trends for β = 0.7 in the submerged jet.

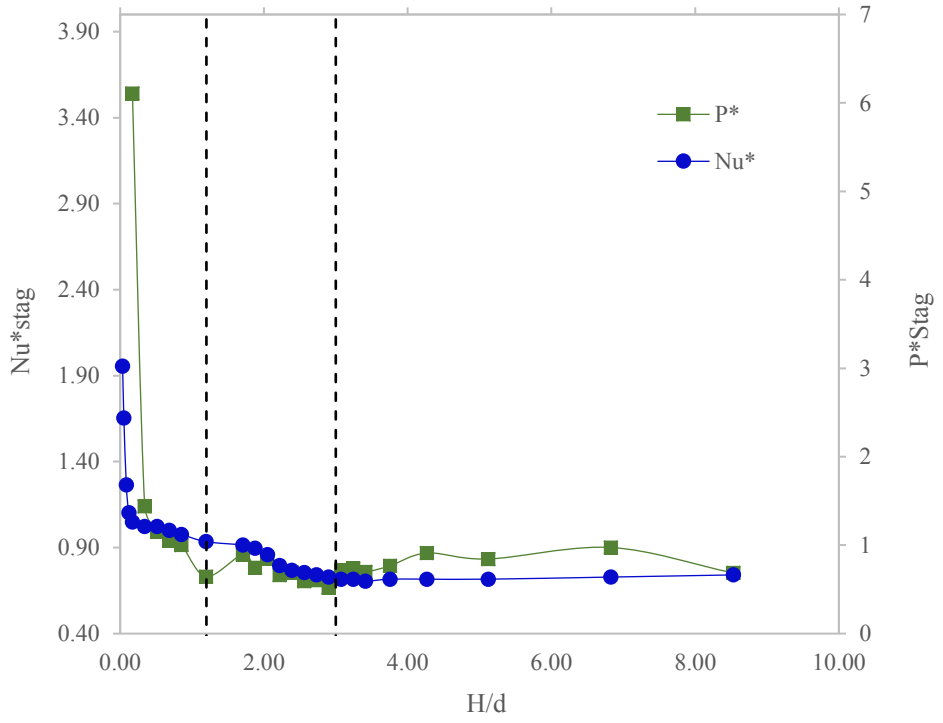

Figure 48: Nusselt number and stagnation pressure trends for β = 0.9 in the free surface jet.

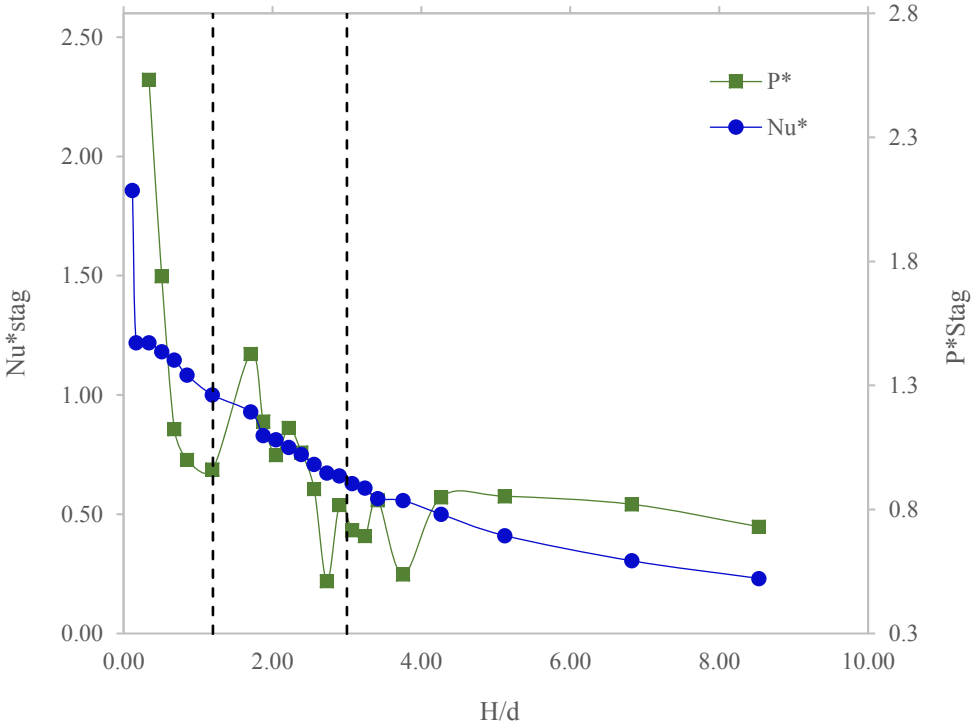

Figure 49: Nusselt number and stagnation pressure trends for β = 0.9 in the submerged jet.

The trends of the Nusselt number and stagnation pressure decreased exponentially in both free surface and submerged jets for all volumetric qualities in Region I. In Region II, the Nusselt number and stagnation pressure of the free surface jet remained constant with some fluctuation. The Nusselt number and stagnation pressure of the submerged jet continued to decrease linearly. In Region III, the Nusselt number and stagnation pressure of the free surface jet increased linearly and the Nusselt number and stagnation pressure of the submerged jet decreased linearly.

4.3.3 Comparison between Free Surface Jet and Submerged Jet

Comparing the values of the free surface and submerged jet, the free surface jet had a higher Nusselt number for low nozzle-to-plate spacings. As the nozzle-to-plate spacing increased, the Nusselt number of the submerged jet decreased linearly while the Nusselt number of the free surface jet increased linearly. At some point, they intersect and the free surface jet Nusselt number becomes larger than that of the submerged jet. The point of intersection varies for each volumetric quality. The nozzle-to-plate spacing at which the intersections occur for each volumetric quality can be found in Table 3. In this table, the nozzle-to-plate spacing values for both the centered thermocouple and the off-set thermocouple are listed for each volumetric quality. The height at which they intersect is low at $\beta = 0.1$ and increased until $\beta = 0.5$ where the height is the highest, and decreased again until $\beta = 0.9$.

Table 3: H/d value at intersection of Nusselt number.

β	Center	Off-set
0.1	0.51	0.68
0.3	2.9	1.19
0.5	5	3.41
0.7	2.73	1.71
0.9	1.71	1.19

The comparison between the free surface and submerged jet for the centered thermocouple can be seen in Figures 50 - 54. The comparison of the two jets for the off-centered jet can be seen in the appendix.

At $\beta = 0.1$, the value of the submerged jet is only larger by a small amount until $H/d = 0.51$. From $2.05 < H/d < 3.24$, the values are almost exactly the same, until the free surface jet increased linearly and the submerged jet decreased linearly. At $\beta = 0.3, 0.5, 0.7$, the submerged jet Nusselt numbers are higher than the free surface jet, and the difference between the two is larger than the difference at $\beta = 0.1$. The largest differences occur when $\beta = 0.5, 0.7$. At $\beta = 0.9$, the differences become small again.

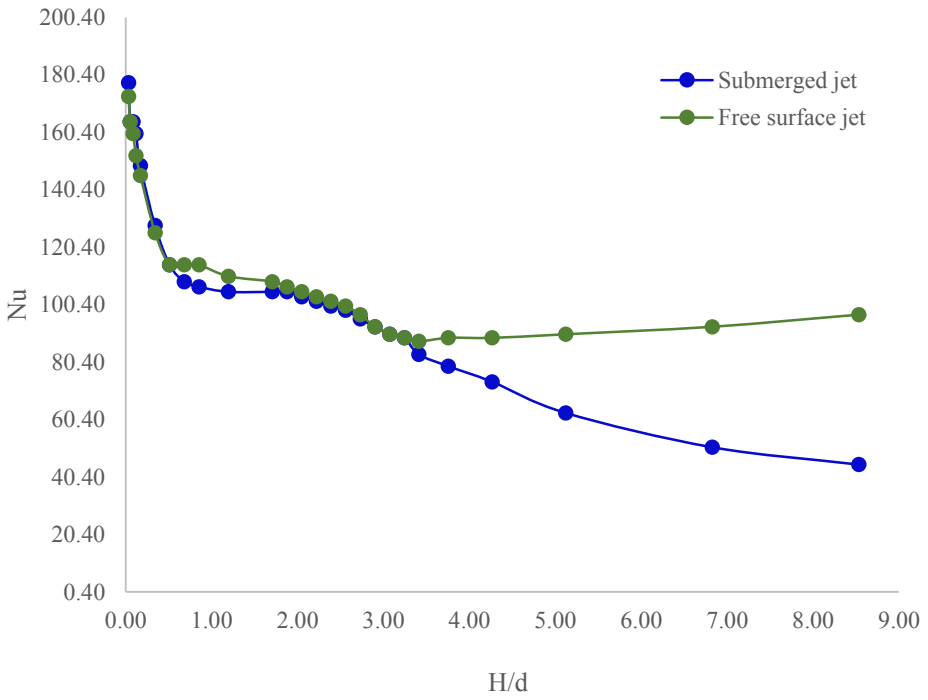

Figure 50: Comparison of Nusselt number between submerged and free surface jet for β = 0.1.

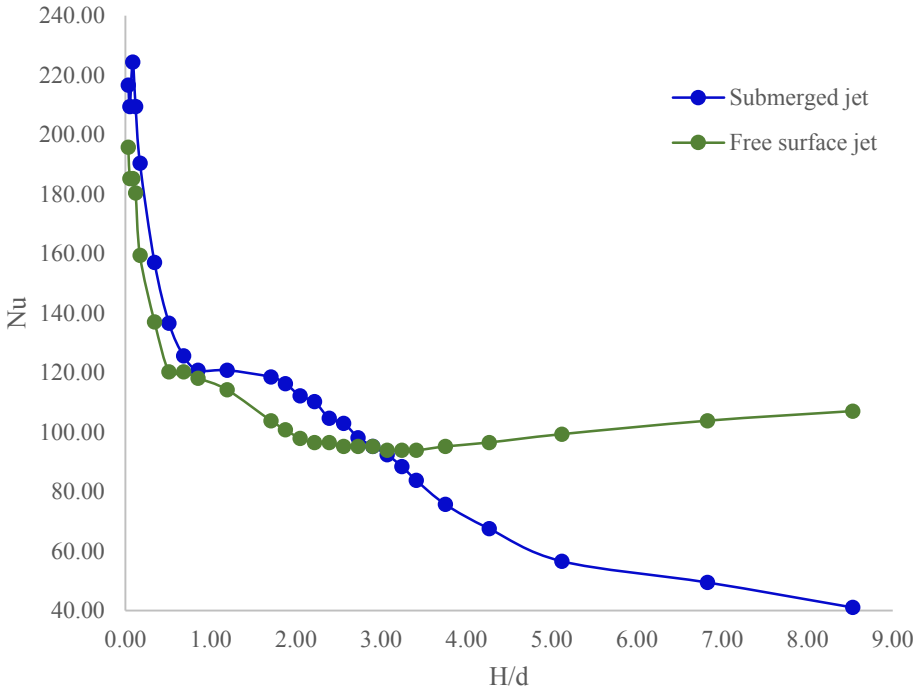

Figure 51: Comparison of Nusselt number between submerged and free surface jet for β = 0.3.

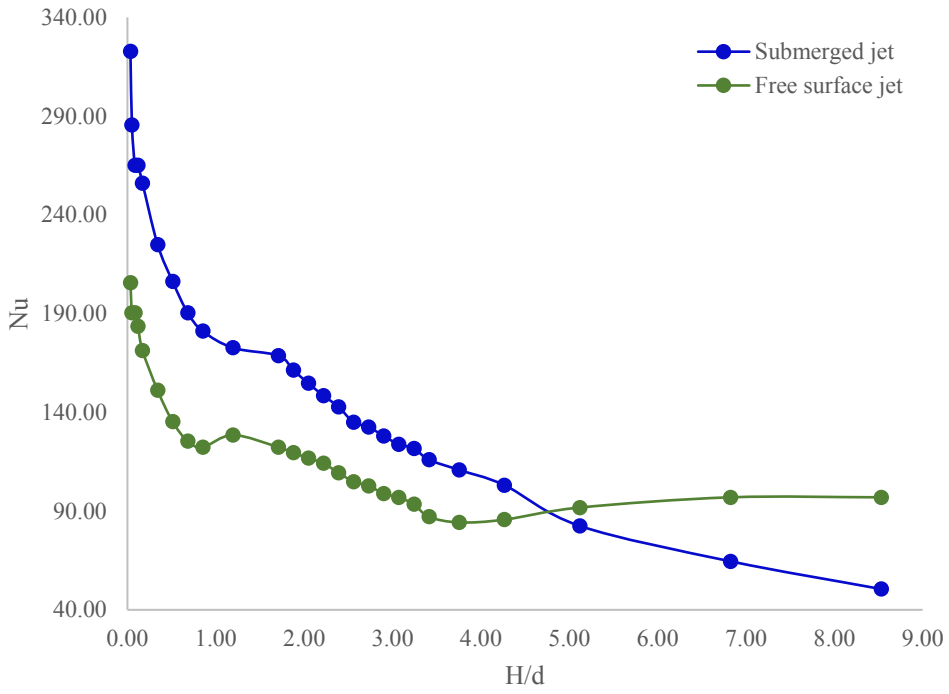

Figure 52: Comparison of Nusselt number between submerged and free surface jet for β = 0.5.

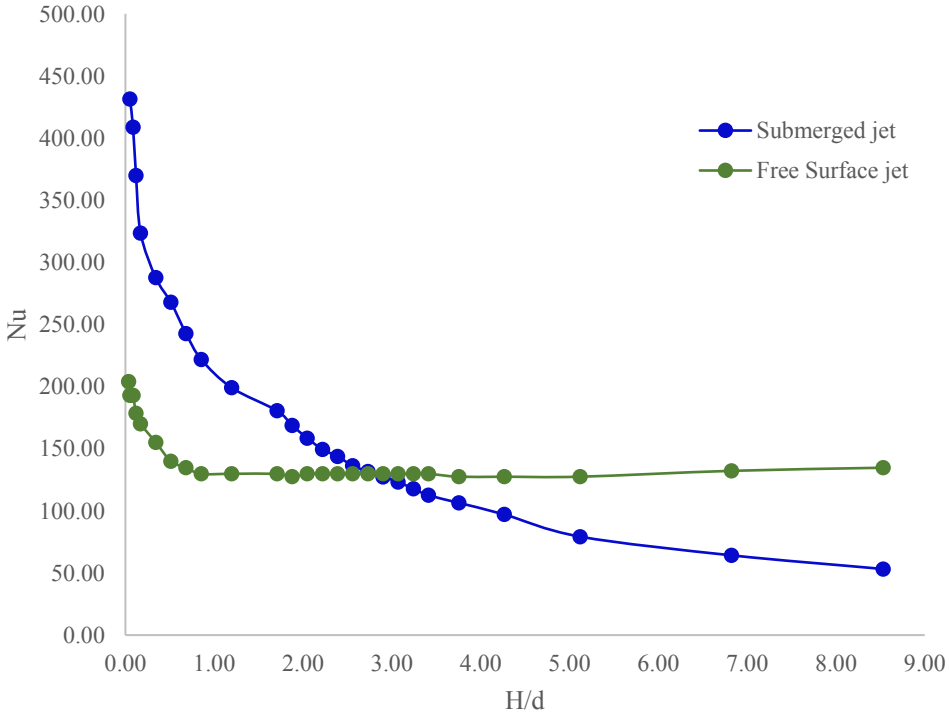

Figure 53: Comparison of Nusselt number between submerged and free surface jet for β = 0.7.

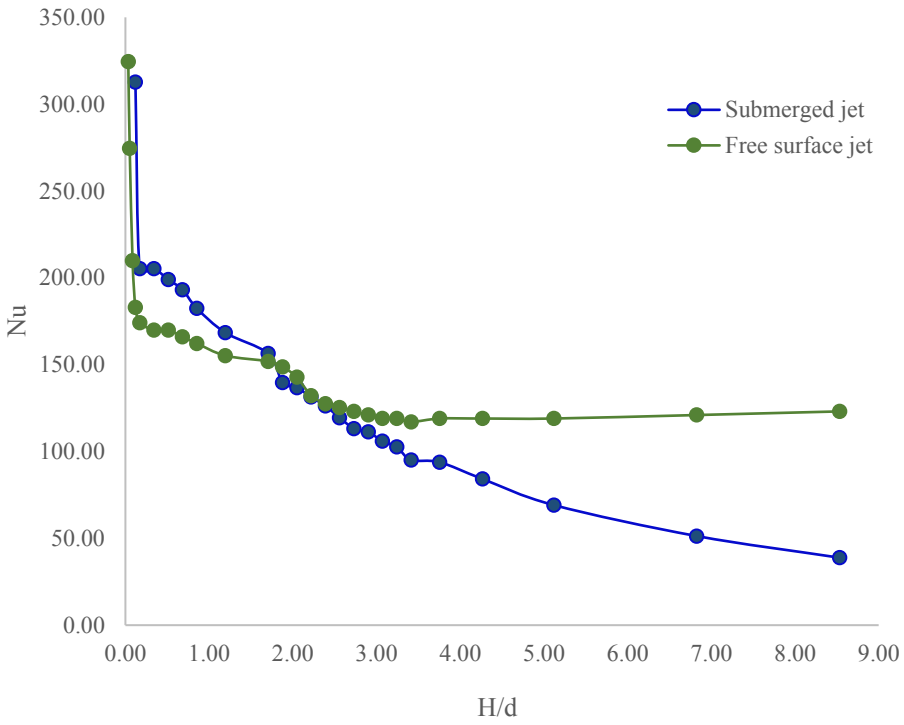

Figure 54: Comparison of Nusselt number between submerged and free surface jet for β = 0.9.

CHAPTER 5

CONCLUSIONS AND FUTURE WORK

The goal of this research was to understand the effects of the nozzle-to-plate spacing and volumetric quality, on the Nusselt number of two-phase, free surface impinging jets and submerged impinging jets. The effects of pressure, and pressure fluctuation were observed. The Nusselt number of two-phase, free surface and submerged impinging jets were obtained at several nozzle-to-plate spacings and the trends were compared to the trends of the pressure. The Nusselt number of the two-phase, submerged jet was also analyzed at several nozzle-to-plate spacing, and the values were compared to those of the free surface jets with the same conditions. The two fluids of the jet were water and air. The nozzle-to-plate spacing ranged from $H/d = 0.03 - 8.5$ and the experiment was done at five volumetric qualities, $\beta = 0.1, 0.3, 0.5, 0.7, 0.9$. The pressure and the fluctuation of the pressure at the stagnation point was also taken into consideration to understand how they affect the heat transfer characteristics.

The Nusselt number and stagnation pressure decreased exponentially in both free surface and submerged jets for all volumetric qualities in Region I, the jet deflection region. In Region II, the transition region, the trends of the Nusselt number and stagnation pressure of the free surface jet remains constant with some fluctuation. The Nusselt number and stagnation pressure of the submerged jet continued to decrease linearly. In Region III, the

Nusselt number and stagnation pressure increased linearly in the free surface jet and decreased linearly in the submerged jet.

Comparing the values of the free surface and submerged jet, the submerged jet has a higher Nusselt number for low nozzle-to-plate spacings. As the nozzle-to-plate spacing increased, the Nusselt number of the submerged jet decreased linearly while the Nusselt number of the free surface jet increased linearly. At some point, they intersect and the free surface jet Nusselt number becomes larger than that of the submerged jet. The point of intersection varies for each volumetric quality. The height at which they intersect is low at $\beta = 0.1$ and increased until $\beta = 0.5$ where the height is the highest, and decreased again until $\beta = 0.9$. At $\beta = 0.1$, the value of the submerged jet is only larger by a small amount until $H/d = 0.51$. From $2.05 < H/d < 3.24$, the values are almost exactly the same, until the free surface jet increased linearly and the submerged jet decreased linearly. At $\beta = 0.3, 0.5, 0.7$, the submerged jet Nusselt numbers are higher than the free surface jet, and the difference between the two is larger than the difference at $\beta = 0.1$. The largest differences occur when $\beta = 0.5, 0.7$. At $\beta = 0.9$, the differences become small again.

The results discussed in this work are not all encompassing. There are still many unanswered questions in regards to two-phase submerged impinging jets. Definition of whether the impinging jet is turbulent or laminar once it exits the nozzle remains unclear. Future work exploring this concept would include finding Nusselt numbers of lateral positions along the heater, and further exploration of the pressure and velocity fluctuation at these positions. Similar experiments on single-phase and free surface jets have been done. As a part of the research done in this work, two thermocouples were used during the heat transfer experiment. The comparison of the Nusselt number of the offset thermocouple

for free surface and submerged jets can be found in the appendix. For each volumetric quality the submerged jet Nusselt number is higher than the free surface jet Nusselt number at low nozzle-to-plate spacings. Just as with the centered thermocouple, the Nusselt number of the submerged jet decreased faster than that of the free surface jet as the nozzle-to-plate spacing increases. Again, each volumetric quality has an intersection point and the point vary similarly to the centered thermocouple. Two thermocouples is not enough to obtain a radial profile of the Nusselt number, and future work would include multiples thermocouples to obtain a radial profile of the Nusselt number and stagnation pressure of free surface and submerged impinging jets.

The trend of the Nusselt number has never been explained in relation to the pressure fluctuation. Recall the study by Gardon and Akfirat [11], where a turbulence promoter increased the heat transfer coefficient of the jet from that obtained with a plain nozzle. The region in which the heat transfer was increased was $1 < H/d < 8$. The trends of the fluctuation and the Nusselt number do not perfectly align in this region, but it is possible that the fluctuation is affecting it. Future work would include comparisons between single-phase, liquid only flow and multiple volumetric qualities. Other future work would also include the effects of pressure fluctuation on Nusselt number.

CHAPTER 6

REFERENCES

[1] B. Han, R.J. Goldstein, "Jet-impingement heat transfer in gas turbine systems," *Ann. N. Y. Acad. Sci.,* vol. 934, p. 147–161, 2001.

[2] S. Polat, B. Huang, A.S. Mujumdar, W.J.M. Douglas, "Numerical flow and heat transfer under imping jets: a review," *Fluid Mech. Heat transfer,* vol. 2, p. 157–197, 1989.

[3] H. Martin, "Heat and mass transfer between impinging gas jets and solid surfaces," *Adv. Heat Transfer,* no. 13, p. 1–60, 1977.

[4] M. Fabbri, S. Jiang, V.K. Dhir, "A comparative study of cooling of high power density electronics using sprays and microjets," *J. Heat Transfer,* vol. 127, p. 38–48, 2005.

[5] J. Lee, S.J. Lee, "The effect of nozzle aspect ratio on stagnation region heat transfer characteristics of elliptic impinging jet," *Int. J. Heat Mass Transfer,* vol. 43, pp. 555-575, 2000.

[6] P. Tie, Q. Li, Y. Xuan, "Investigation on the submerged liquid jet arrays impingement cooling," *Applied Thermal Engineering,* vol. 31, pp. 2757-2763, 2011.

[7] K. Choo, Sung Jin Kim, "Heat transfer and fluid flow characteristics of two-phase impinging jets," *International Journal of Heat and Mass Transfer,* vol. 53, pp. 5692-5699, 2010.

[8] S.J. Freidman, A.C. Mueller, "Heat transfer to flat surfaces," in *The General Discussion on Heat Transfer*, London, 1951.

[9] R. Gardon, J. Cobonpue, "Heat transfer between a flat plate and jets of air impinging on it," *Int. Developments in Heat Transfer, ASME, New York,* p. 454–460, 1962.

[10] G. M. Carlomagno, A. Ianiro, "Thermo-fluid-dynamics of submerged jets impinging at short nozzle-to-plate distance: A review," *Experimental Thermal and Fluid Science,* vol. 58, pp. 15--25, 2014.

[11] R. Gardon, J.C. Akfirat, "The role of turbulence in determining the heat transfer characteristics of impinging jets," *Int. J. Heat Mass Transfer,* vol. 8, p. 1261–1272, 1965.

[12] S. Eiamsa-ard, K. Nanan, K. Wongcharee, "Heat transfer visualization of co/counter-dual swirling impinging jets by thermochromic liquid crystal method," *International Journal of Heat and Mass Transfer,* vol. 86, pp. 600-621, 2015.

[13] U. Ansu, S. C. Godi, A. Pattamatta, C. Balaji, "Experimental investigation of the inlet condition on jet impingement heat transfer using liquid crystal thermography," *Experimental Thermal and Fluid Science,* vol. 80, pp. 363-375, 2016.

[14] R.J. Goldstein, J.F. Timmers, "Visualization of heat transfer from arrays of impinging jets," *Int. J. Heat Mass Transfer,* vol. 25, p. 1857–1868, 1982.

[15] H. Li, S. Chao, G. Tsai, "Thermal performance measurement of heat sinks with confined impinging jet by infrared thermography," *International Journal of Heat and Mass Transfer,* vol. 48, p. 5386–5394, 2005.

[16] V. Chaugule, R. Narayanaswamya, A. D. Lucey, V. Narayanan, J. Jewkes, "Particle image velocimetry and infrared thermography of turbulent jet impingement on an oscillating surface," *Experimental Thermal and Fluid Science,* vol. 98, pp. 576-593, 2018.

[17] T. Astarita, G.M. Carlomagno, "Infrared Thermography for Thermo-fluid-dynamics," in *Springer-Verlag*, Berlin, 2013.

[18] G.M. Carlomagno, L. de Luca, "Infrared thermography for flow visualization and heat transfer measurements," in *Workshop Stato dell'arte del rilevamento con camera termiche nella banda 8–15 micron*, Firenze, 1991.

[19] D. Lytle, B.W. Webb, "Air jet impingement heat transfer at low nozzle-plate spacings," *Int. J. Heat Mass Transfer,* no. 37, p. 1687–1697, 1994.

[20] C.C. Landreth, R.J. Adrian, "Impingement of a low Reynolds number turbulent circular jet onto a flat plate at normal incidence," *Exp. Fluids,* vol. 9, pp. 74-84, 1990.

[21] E. Baydar, "Confined impinging air jet at low Reynolds numbers," *Exp. Therm. Fluid Sci.,* vol. 19, pp. 27-33, 1999.

[22] M.J. Tummers, J. Jacobse, S.G. Voorbrood, "Turbulent flow in the near field of a round impinging jet," *Int. J. Heat Mass Transfer,* vol. 54, p. 4939–4948, 2011.

[23] K. J. Hammad, I. Milanovic, "Flow Structure in the Near-Wall Region of a Submerged Impinging Jet," *Journal of Fluids Engineering,* vol. 133, 2011.

[24] M. Modak, K. Garg, S. Srinivasan, S. K. Sahu, "Theoretical and experimental study on heat transfer characteristics of normally impinging two dimensional jets on a hot surface," *International Journal of Thermal Sciences,* vol. 122, pp. 174-187, 2016.

[25] J.A. Schetz, A.E. Fuhs, Fundamentals of Fluid Mechanics, New York: John Wiley & Sons, 1999.

[26] J.N.B. Livingood, P. Hrycak, "Impingement heat transfer from turbulent air stream jets to flat plates-a literature survey," NASA TM X-2778, Lewis Research Center, 1973.

[27] H. Schrader, "Trocknung Feuchter dberfllchen Mittels Warmluftstrahlen; StrSmungsvorgZinge und Stoffiibertragung, Forschungsh," *Ver. Dtsch. Zg.,* p. 484, 1961.

[28] A. Leclerc, "Deviation d'un jet liquide par une plaque normale 8 son axe," *Ho&e Blanche,* pp. 816-821, 1950.

[29] M. Glauert, "The wall jet," *J. Fluid Mech.,* vol. 1, pp. 625-643, 1956.

[30] G.N. Abramovich, L.H. Schindel, "The Theory of Turbulent Jets," *MIT Press,* 1984.

[31] K. Choo, B. K. Friedrich, A. W. Glaspell, K. A. Schilling, "The influence of nozzle-to-plate spacing on heat transfer and fluid flow," *International Journal of Heat and Mass Transfer,* vol. 97, pp. 66-69, 2016.

[32] D.A. Zumbrunnen, M. Balasubramanian, "Convective heat transfer enhancement due to gas injection into an impinging liquid jet," *ASME J. Heat Transfer,* vol. 117, p. 1011–1017, 1995.

[33] A. Serizawa, O. Takahashi, Z. Kawara, T. Komeyama, I. Michiyoshi, "Heat transfer augmentation by two-phase bubbly flow impinging jet with a confining wall," in *9th Int. Heat Transfer Conference*, Jerusalem, 1990.

[34] B. K. Friedrich, A. W. Glaspell, K. Choo, "The effect of volumetric quality on heat transfer and fluid flow characteristics of air-assistant jet impingement," *International Journal of Heat and Mass Transfer,* vol. 101, pp. 261-266, 2016.

[35] D. Trainer, "Effects of flow pattern on the breakup length of cicular air-assisted water jets," *Atomization and Sprays,* vol. x(x), p. 1–25, 2018.

[36] D.E. Hall, F.P. Incropera, R. Viskanta, "Jet impingement boiling from a circular free surface jet during quenching; Part 2 – Two-phase jet," *ASME J. Heat Transfer,* vol. 123, pp. 911-917, 2001.

[37] C.T. Chang, G. Kojasoy, F. Landis, S. Downing, "Confined single- and multiple-jet impingement heat transfer – II. Turbulent two-phase flow," *Int. J. Heat Mass Transfer,* vol. 38, p. 843–851, 1995.

[38] R. Viskanta, "Heat transfer to impinging isothermal gas and flame jets," *Exp. Therm. Fluid Sci.,* vol. 6, p. 111–134, 1993.

[39] S. Polat, "Heat and mass transfer in impingement drying," *Dry. Technol.,* vol. 11, p. 1147–1176, 1993.

[40] S. Corrsin, "Investigation of flow in an axially symmetrical heated jet of air," NACA Wartime Reports W-94, Washington, 1943.

[41] K.J. McNaughton, C.G. Sinclair, "Submerged jets in short cylindrical flow vessels," *J. Fluid Mech.,* vol. 25, p. 367–375, 1996.

[42] H. M. Hofmann, M. Kind, H. Martin, "Measurements on steady state heat transfer and flow structure and new correlations for heat and mass transfer in submerged impinging jets," *International Journal of Heat and Mass Transfer,* vol. 50, pp. 3957-3965, 2007.

[43] F. M. White, Fluid Mechanics, New York: McGraw-Hill, 2003.

APPENDIX: OFF-CENTERED JET CASES

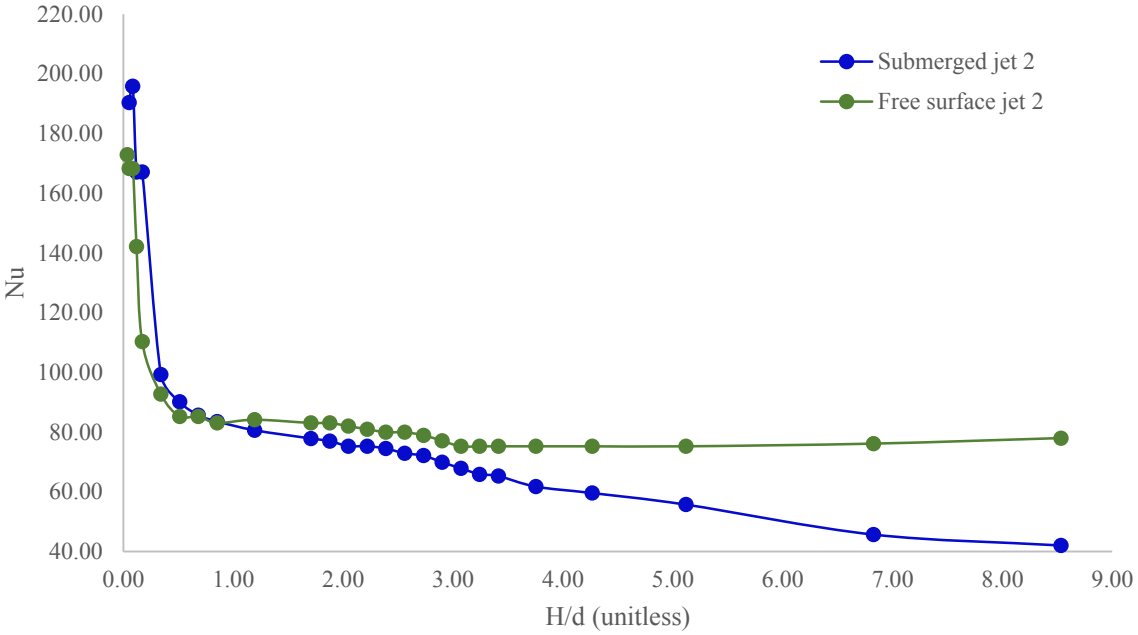

Figure 55: Comparison between submerged and free surface jet for β = 0.1.

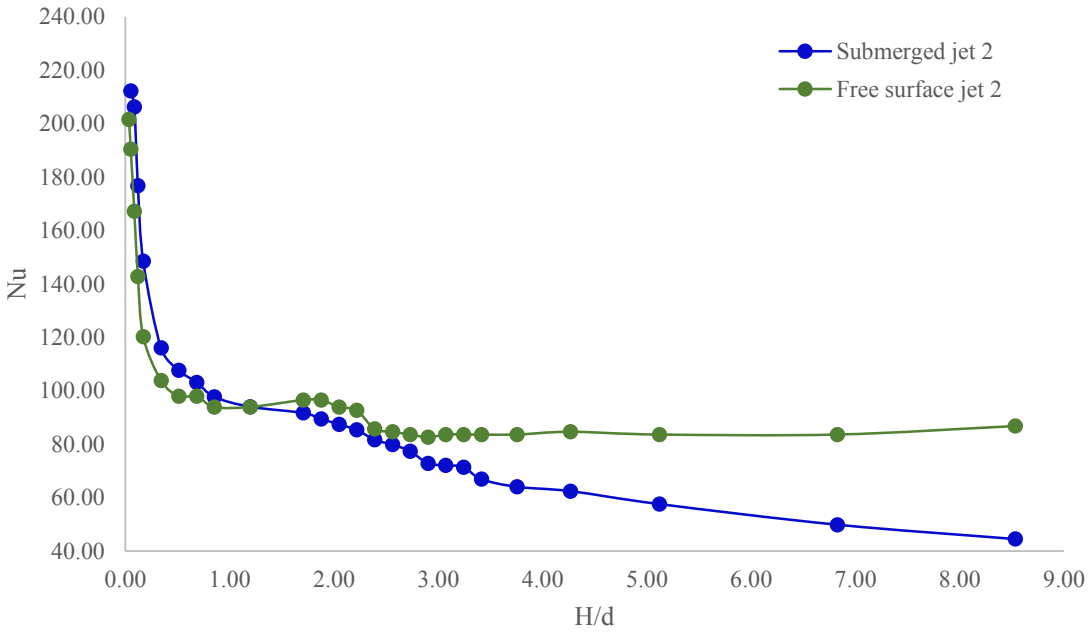

Figure 56: Comparison between submerged and free surface jet for β = 0.3.

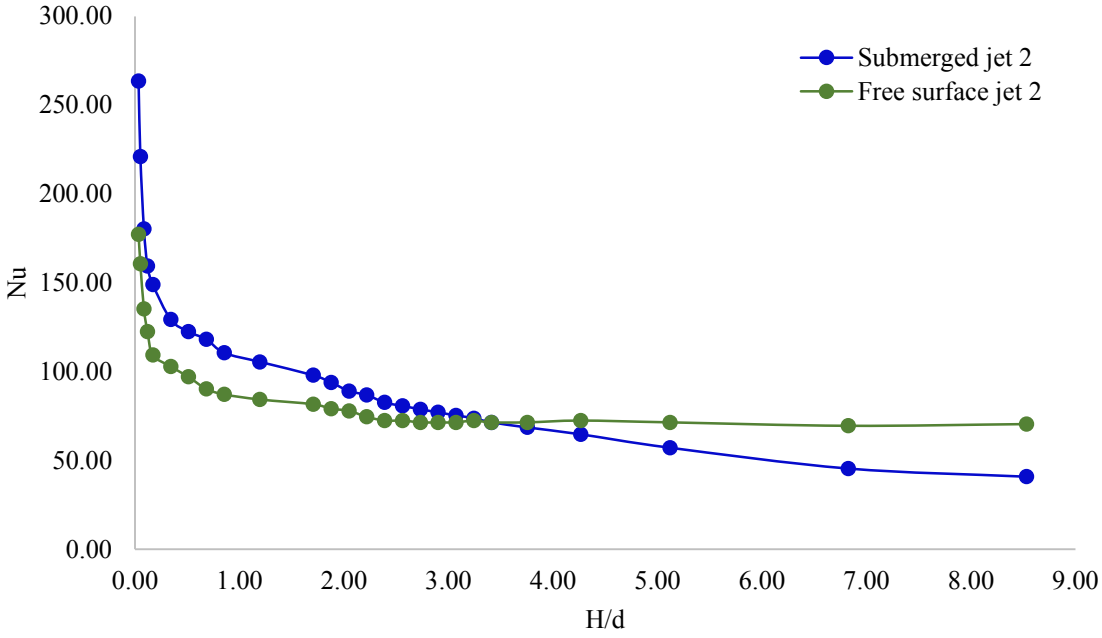

Figure 57: Comparison between submerged and free surface jet for β = 0.5.

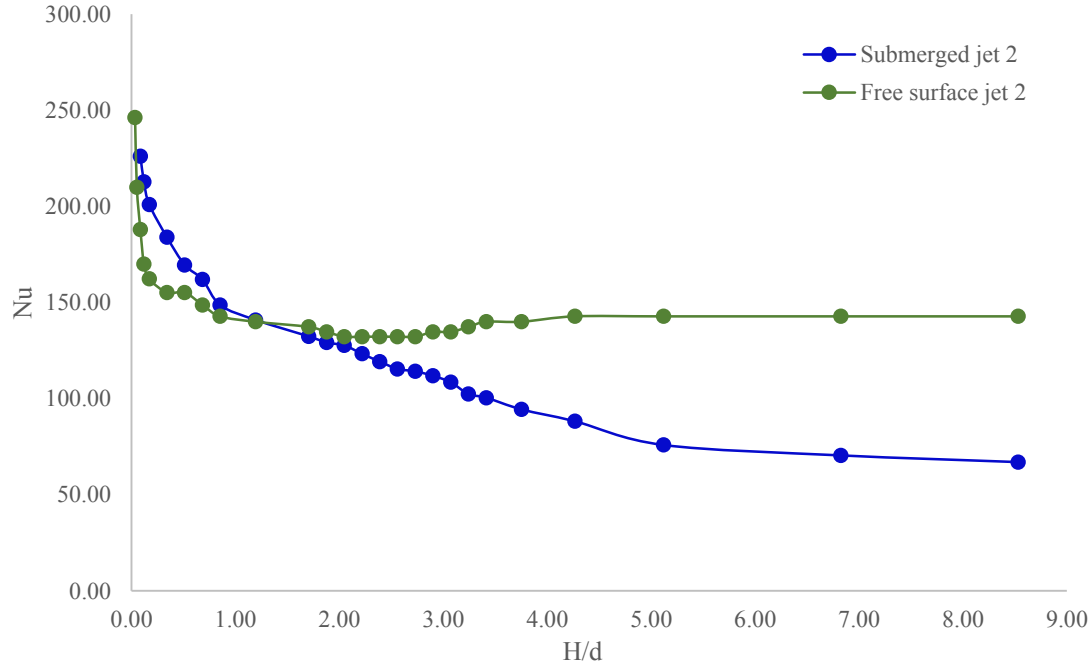

Figure 58: Comparison between submerged and free surface jet for β = 0.7.

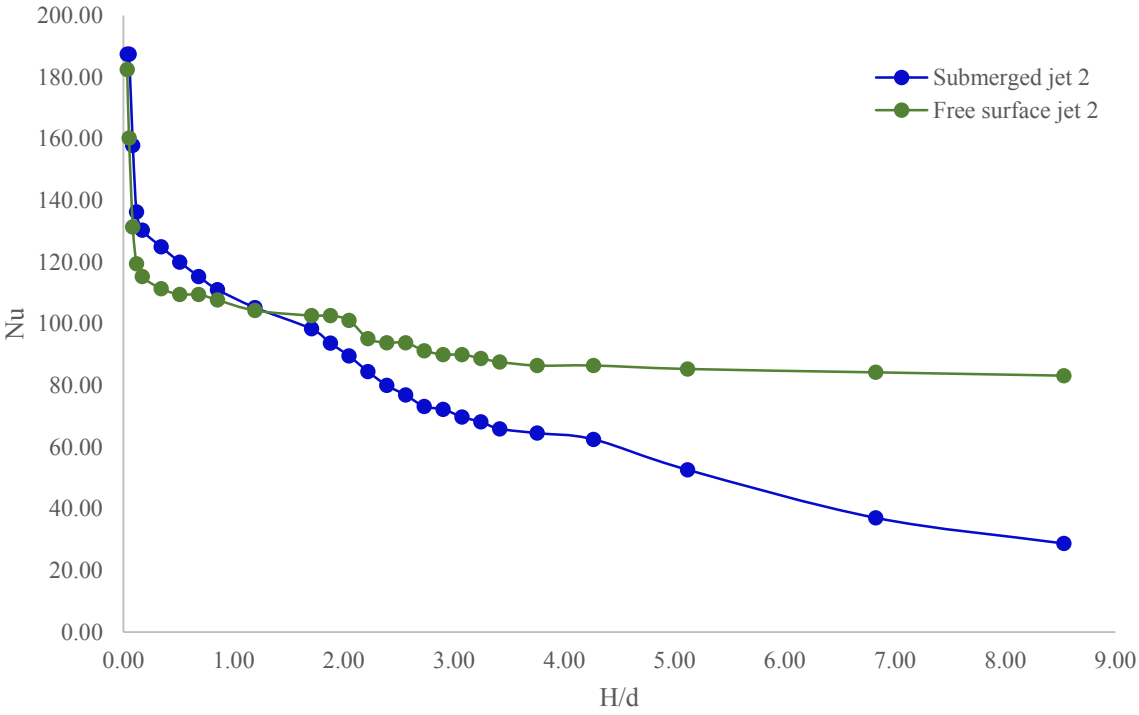

Figure 59: Comparison between submerged and free surface jet for β = 0.9.